ENETS Consensus Guidelines for the Standards of Care in Neuroendocrine Tumors

DOI:
10.1159/000471879

Document Version
Accepted author manuscript

Neuro endocrinology

Neuroendocrinology (DOI:10.1159/000471879)
(Accepted, unedited article not yet assigned to an issue)

Advanced Release: March 30, 2017

Received: December 5, 2016
Accepted after revision: March 21, 2017

ENETS Consensus Guidelines for the Standards of Care in Neuroendocrine Tumors: Radiological, Nuclear Medicine & Hybrid Imaging

Anders Sundin[1], Rudolf Arnold[2], Eric Baudin[3], Jaroslaw B Cwikla[4], Barbro Eriksson[5], Stefano Fanti[6], Nicola Fazio[7], Francesco Giammarile[8], Rodney J. Hicks[9], Andreas Kjaer[10], Eric Krenning[11], Dik Kwekkeboom[12], Catherine Lombard-Bohas[13], Juan M O´Connor[14], Dermot O´Toole[15], Andrea Rockall[16], Bertram Wiedenmann[17], Juan W Valle[18], Marie-Pierre Vullierme[19], all other Antibes Consensus Conference participants

[1] Anders Sundin, Department of Radiology, Inst. Surgical Sciences, Uppsala University, Uppsala, Sweden;

[2] Rudolf Arnold, Department of Gastroenterology and Endocrinology, Philipps University, Marburg, Germany;

[3] Eric Baudin, Endocrine Oncology and Nuclear Medicine, Gustave Roussy, Villejuif, France;

[4] Jaroslaw B Cwikla, Department of Radiology, Faculty of Medical Sciences, University of Warmia and Mazury Olsztyn, Poland;

[5] Barbro Eriksson, Department of Medical Sciences, Uppsala University, Uppsala, Sweden;

[6]Stefano Fanti, Nuclear Medicine Policlinico S.Orsola, University of Bologna, Bologna, Italy;

[7] Nicola Fazio, Unit of Gastrointestinal Medical Oncology and Neuroendocrine Tumors, European Institute of Oncology, Milan, Italy;

[8] Francesco Giammarile, Nuclear Medicine Department, Hospices Civils de Lyon and EMR3738, University of Lyon, France:

[9] Rodney J. Hicks, Cancer Imaging, the Peter MacCallum Cancer Centre, Melbourne, Australia

[10] Andreas Kjaer, Department of Clinical Physiology, Nuclear Medicine & PET and Cluster for Molecular Imaging, Rigshospitalet and University of Copenhagen, Denmark

[11] Eric Krenning, Department of Nuclear Medicine, Erasmus MC, Rotterdam, The Netherlands;

[12] Dik Kwekkeboom, Department of Nuclear Medicine, Erasmus MC, Rotterdam, The Netherlands;

[13] Catherine Lombard-Bohas, Institut du Cancer, Hospices Civils de Lyon, Hôpital E Herriot, Lyon, France;

[14] Juan Manuel O´Connor, Alexander Fleming Institute, Gastroenterology Hospital B. Udaondo, Buenos Aires Argentina;

[15] Dermot O´Toole, Trinity College Dublin, University of Dublin, St James's Hospital and St Vincent's University Hospital, Dublin;

[16] Andrea Rockall, Department of Radiology, The Royal Marsden NHS Foundation Trust, and Imperial College London;

[17] Bertram Wiedenmann, Dept. of Hepatology and Gastroenterology, Campus Charité Mitte & Campus Virchow-Klinikum, Charité – Universitaetsmedizin Berlin, Berlin, Germany;

[18] Juan W Valle, Institute of Cancer Sciences, University of Manchester / The Christie NHS Foundation Trust, Manchester, UK;

[19] Marie-Pierre Vullierme, Service de Gastroentérologie,Hôpital Beaujon, Clichy, France;

Corresponding author:

Anders Sundin

Department of Radiology

Inst. Surgical Sciences

Uppsala University

Uppsala University Hospital,

SE-751 85 Uppsala, Sweden

Email : anders.sundin@radiol.uu.se

Telephone : +46-18-611 93 48

Abstract

Contrast-enhanced computed tomography (CT) of the neck-thorax-abdomen and pelvis, including three-phase examination of the liver, constitutes the basic imaging for primary NET diagnosis, staging, surveillance and therapy monitoring. CT characterization of lymph nodes is difficult because of inadequate size criteria (short axis diameter), and bone metastases are often missed. Contrast-enhanced magnetic resonance imaging (MRI) including diffusion-weighted imaging is preferred for examination of the liver, pancreas, brain and bone. MRI may miss small lung metastases. MRI is less

well suited than CT for examination of extended body areas, because of the longer examination procedure. Ultrasonography (US) frequently provides the initial diagnosis of liver metastases and contrast-enhanced US is excellent to characterize liver lesions that remain equivocal on CT/MRI. US is the method of choice to guide the biopsy needle for the histopathological NET diagnosis. US cannot visualize thoracic NET lesions for which CT guided biopsy therefore is used. Endocopic US is the most sensitive method to diagnose pancreatic NETs, and additionally allows for biopsy. Intraoperative US facilitates lesion detection in the pancreas and liver. Somatostatin receptor imaging should be a part of the tumor staging, preoperative imaging and re-staging, for which ^{68}Ga-DOTA-somatostatin analog-PET/CT is recommended, which is vastly superior to somatostatin receptor scintigraphy, and facilitates diagnosis of most types of NET lesions, for example lymph node metastases, bone metastases, liver metastases, peritoneal lesions and primary small-intestinal NETs.^{18}FDG-PET/CT is better suited for G3 and high G2 NETs, which generally have higher glucose metabolism and less somatostatin receptor expression than low grade NETs.

Introduction

The vast majority of neuroendocrine tumors (NETs) are well differentiated and slow-growing with only a minority showing a clinically aggressive behavior. NETs can produce a variety of metabolically active substances (hormones and amines) leading to distinct clinical syndromes (functioning tumors). However, the majority are non-functioning and present either with locally advanced disease, giving rise to site-specific symptoms, or distant metastases, mainly to the liver.

These various distinct features in tumor growth, secretory capacity and anatomical localisation are reflected in the wide variation in clinical presentation of different NETs. Consequently, the need for diagnostic procedures and the choice of imaging methods varies considerably depending on the patient's tumor status at presentation. The various imaging aspects to consider in the choice of radiological and nuclear medicine imaging methods are related to primary tumor detection, evaluation of its local extent and relation to adjacent anatomical structures, staging of the tumor concerning regional and distant metastases, evaluation of tumor somatostatin receptor density, therapy monitoring and detection of recurrent disease.

Materials and Methods

This is an update of the first ENETS Consensus Guidelines for the Standards of Care in NeuroendocrineTumors: Radiological Examinations [1] and Receptor Imaging with ^{111}In-Pentetreotide [2] and a fusion of the two papers into one publication comprising radiological and nuclear medicine imaging. This reflects the rapidly increasing and complementary role of hybrid imaging techniques whereby computed tomography (CT) is performed together with nuclear medicine procedures. Current positron emission tomography (PET) and Single Photon Computed Emission Tomography (SPECT) systems generally include a CT scanner, which allow a fully diagnostic CT to be acquried and fused as PET/CT or SPECT/CT images.

The participants of the ENETS scientific advisory board working group, which also included **members** of the European Association of Nuclear Medicine (EANM) **and the European Society of Radiology (ECR),** considered the use of radiological and nuclear medicine imaging methods for the various NET imaging applications in relation to published literature on imaging efficacy together with the expertise of the participants and taking the availability of the various modalities into account. Further aspects considered were patient preparation and information, clinical information needed to optimise imaging technique and image interpretation, examination protocols, reporting of image findings and radiation dose to the patient.

Comparisons of results in the NET imaging literature were hampered by variable reporting of results and differing patient populations. While imaging sensitivity, which is calculated with reference to a putative gold standard such as pathology, this is often not feasible in patients with widely metastatic disease. Therefore, many studies have resorted to reporting the lesion detection rate, which merely states the proportion of patients with disease that is detected by the imaging method out of all examined subjects. Comparisons between studies may also be difficult because imaging results are sometimes based on a patient-by-patient analysis whereas others show lesion-by-lesion based results.

Studies were only considered for reference when they used current standards of imaging. Thus, non-spiral (helical) CT studies, trials on CT without adequate contrast enhancement, and MRI studies that utilized low field strength (<0.5 T) were excluded as well as studies using stand-alone SPECT and stand-alone PET (non-hybrid imaging).

Results

Computed Tomography

Spiral (helical) CT has been the standard technique for many years and modern multidetector CT (MDCT) scanners are now available in the radiology departments. By utilising a large number of parallel detector rows and an X-ray tube rotation time of 0.3–0.5 s, hundreds of ≤1-mm transversal images are acquired per second and the whole abdomen and thorax may be examined during one breath hold. These thin, detailed images may be reformatted in any chosen anatomical plane, usually in the transverse, coronal and sagittal views so called multiplanar reconstructed images (MPR) with isotropic resolution. The thin images also allow reconstruction in three-dimensional (3D) volumes that can be rotated to appreciate anatomy and pathological findings better. Importantly, the fast MDCT technique allows the use of intravenous contrast media with acquisition in several contrast-enhancement phases. MDCT has therefore developed as one of the central techniques for oncological imaging including NETs.

A recent development is the simultaneous detection of X-rays with different energy, so called dual energy CT (DECT), whereby either two X-ray tubes are used simultaneously at different tube potential (typically 80kV and 140kV) or one X-ray tube switches between two different tube tensions during scanning. The X-ray attenuation of a tissue depends on the tube tension during scanning. The attenuation difference at the high and low tube tension, respectively, is larger for a high attenuating tissue than for a low attenuation tissue. A low X-ray tube tension may be applied to better utilize iodine (with high attenuation) based contrast media, either to yield better contrast-enhancement at the same contrast medium dose and/or achieve the same contrast-enhancement at a lower dose. Simultaneous high and low X-ray tube tension at scanning during intravenous contrast-enhancement also allows for post processing whereby the contrast medium may be subtracted to achieve “virtual pre-contrast images”. DECT is currently also investigated for its role in tissue characterization.

Sensitivity, Specificity and Detection Rate

The CT-acquired sensitivity, specificity and detection rate (mean and range based on the number of patients and studies) for various NETs is presented in Table 1. The number of dedicated spiral CT and MDCT studies is limited; therefore CT imaging results from comparative somatostatin receptor imaging trials (scintigraphy and PET) are included in the present data. The sensitivity and specificity for CT to detect patients with NET ranges 61-93% and 71-100%, respectively; and the lesion based sensitivity and specificity, ranges 77-85% and 71-85%, respectively [3-6]. For CT diagnosis of a pancreatic NET (pNET) the lesion detection rates ranges 69-94% [7-9] and 67% sensitivity was reported in one study

[10] and 96% in another including patients with von Hippel-Lindau disease [11]. CT sensitivity for NET liver metastases ranges 75-100% [3,12-15] and specificity 83-100% [10,12,14,15].
Notably, one study used a different methodology and compared thin slice histopathology after hemihepatectomy correlated with the imaging results; the group reported a CT detection rate of 21% for the 1-70 mm liver metastases [16]. Interestingly, the results for MRI and contrast-enhanced US were also poor with a 33% and 22% lesion detection rate, respectively. This emphasizes the limitations of reporting sensitivity in a disease where there is likely to be micro-metastases below the level of detection by the current imaging techniques. Thus, any report of diagnostic accuracy is highly dependent on the compartor used.

For lymph node metastases CT shows 60-70% sensitivity and 87-100% specificity [13,15,17]. For other soft tissue metastases a 62-67% sensitivity and 98-100% specificity has been reported for CT [3,12,14]. CT sensitivity for bone metastases is varying 46-80% but the specificity is high 98-100% [3,18-19].

CT enteroclysis has shown a 50% to 85 % sensitivity and 25% to 97% specificity for detection of the primary NET in the small bowel [20]. In 219 patients with small bowel tumours, including 19 small bowel NETs (SI-NETs), CT enteroclysis showed a sensitivity and specificity of 85% and 97% respectively [21].

Hard- and Software Requirements

For examination of the abdomen, thorax and neck, the MDCT scanner should allow for acquisition of ≤ 1mm slices in order to reconstruct transverse images at preferably (2-3 mm) slice thickness. The high spatial resolution of the thin slices is needed for optimal examination, especially of the pancreas, liver and neck region. A high temporal resolution is also needed in order to perform examinations in the various contrast-enhancement phases required for proper examination for example of the liver and pancreas.

The software needed for image reconstruction and for multiplanar reconstructed images (MPRs) and 3D maximum intensity projections (MIPs) are generally supplied with the CT scanner. Specialised image post-processing to create volume-rendering technique (VRT) 3D images and virtual endoscopy

images may need additional software programs. Most image workstation software, including those in most current picture archiving and communication systems (PACS) currently allow for reformatting the original ≤1 mm images in any slice thickness, usually 2-3 mm, in the transverse, coronal and sagital planes.

Patient Information

For optimal patient cooperation and examination results, the patient should be well informed and properly prepared. Patients should receive information accordingly to local protocols and practices and these should also refect the type and purpose of the examination.

For most CT procedures, the examination generally takes about 15 min. For abdominal CT, patients need to arrive at the department 1.5 hours in advance of the scan time for filling of the bowel by drinking **approximately** 800 ml of fluid, usually tap water. The patients are placed on the examination bed and moved into a short tunnel, i.e. the CT gantry. During intravenous (i.v) contrast medium (CM) administration the patients initially may experience a feeling of warmth and occasionally the sensation of urinary urgency. A previous history of renal impairment or i.v. CM-related adverse reactions should be checked, whether the reaction was systemic or localized and regarding the CM responsible. Fluids but no solid food is recommended during 12 h before the examination. In patients with impaired renal function it is of particular importance to inform the patient that he or she needs to be well hydrated before the examination in order to reduce the risk of adverse CM-related renal effects. Information on the radiation dose is generally not necessary for the patient. However, it should be documented on the imaging report, according to the local regulatory authorities.

Patient Preparation

For patients having experienced a moderate or severe CM-related reaction by a modern non-ionic and low-osmolar CM, another imaging technique should be considered (MRI, US or hybrid imaging without contrast). If CT is considered to be imperative, another CM should be used since the choice of another modern non-ionic and low-osmolar CM may not cause similar side effects. However, the patient should be pretreated with oral cortison and antihistamine given 12 and 2 hours before contrast medium injection [22] and medical reusucitation personel must be available should anaphylaxis occur. Medications should start 12 hours before the injection; for urgent contrast-enhanced CT examinations

i.v. drug administration is preferred. Also, the type of CM responsible for a previous or current CM-related reaction should, if this information is available, be documented in the radiological report. Further use of this particular CM may then be avoided since the CM-related side effect may be related to the specific CM molecule, and not to iodine-based CM in general. A similar CM by another manufacturer may therefore not produce these adverse events, or the side effects may be less severe. Diabetic patients treated with metformin should stop the drug the day before, or at the latest, the same day as the CM administration and have serum creatinine checked before restarting metformin. In the elderly and low body weight patients, serum creatinine should be interpreted with caution; in such cases creatinine clearance can be used instead (normally >40ml/min). A serum creatinine ≥130 µmol/l puts patients at risk of renal impairment. In such cases hydration with at least 1 litre of fluid before and after CM injection is advised. When serum creatinine is ≥180 µmol/l or creatinine clearance <30ml/min, CT examination is generally performed without i.v. contrast-enhancement. As an aid, various electronic algorithms/computer software are available to estimate the creatinine clearance using the patient's serum creatinine, weight, age and sex as input parameters.

In order to distend the bowel, patients generally drink about **800 ml** of tap water for 1.5 h before an abdominal CT examination. Twenty ml of CM (300–400 mgI/ml) may be added to the tap water when a positive CM filling of the bowel lumen is required (if for example a gastrointestinal tract fistula is suspected). However, for CT examination of NETs, particularly of the pancreas or when duodenal disease is suspected, the duodenum needs to be filled with water without addition of an iodine-based CM. This is best achieved by 150–200 ml of oral water a few minutes before the CT examination. Administration of an anti-peristaltic agent (e.g. butylscopolamine 20 mg i.v.) to reduce bowel motility is optional.

For abdominal CT of the small bowel, CT enteroclysis, distension of the bowel requires a larger fluid volume, approximately 2000 ml. The patient can either drink this during the hour preceeding the examination (hyperosmolar fluid such as mannitol, with a 50% concentration is optimal) or, alternatively the fluid (warm tap water) can be administered through a naso-gastro-jejunal tube. By using a dedicated (150 ml/min rate) power injector, optimal filling of the whole small bowel may be achieved during enteroclysis. CT enteroclysis is performed during i.v. contrast-enhancement, aiming to demonstrate a hypervascular small bowel NET delineated by water in the bowel lumen.

CT of the colon is performed similarly as examination for suspected colonic carcinoma, using a CT colonography technique, with cleaning the bowel and insufflating air or CO2 and requires i.v. contrast-enhancement.

Information Provided by the Clinician

In order to perform a proper CT examination and to decrease potential risks, it is necessary that the referring clinician provides adequate information. This includes the precise diagnosis, current medical therapy, previous surgery and information regarding the presence of diabetes (including use of metformin), renal impairment and previous CM-related adverse reactions. The results of previous imaging examinations are mandatory.

Imaging Technique

The imaging protocols used for CT of the abdomen, including the liver and pancreas, thorax and neck vary slightly according to local experience and routines. Given that the previously recommended hardware requirements are taken into consideration and that bolus-tracking technique is available, various examination protocols usually result in equally good examinations. Consequently, this consensus document is focused on basic examination parameters, instead of detailed protocols, and important general imaging aspects are discussed. For MDCT of the abdomen, thorax and neck ≤1-mm slice thickness and a pitch of 1.25–1.5 is recommended. The pitch is the table movement per tube rotation divided by the width of the total number of the detectors used. The resulting ≤1-mm transaxial images should preferably be reformatted in 2-3 mm MPRs in the transverse, coronal and sagittal planes using a 30-50% overlap. In patients with adequate renal function, i.v. CM is administered. For i.v. contrast-enhancement of the abdomen, 1.5–2 ml/kg body weight (maximum 180 ml) 300–350 mg/ml non-ionic low- or iso-osmolar contrast material should be used at ≥5 ml/s injection rate, using a power injector. A lower injection rate may sometimes be necessary depending on the patients´venous access. The use of a dual syringe injector is recommended by which a 40-80 ml injection of physiological saline can be administered immediately after the CM injection. This assures that the whole CM volume is utilized for contrast-enhancement purposes and it decreases the otherwise undesirably high CM concentration in the brachiocephalic vein and the superior vena cava, which can obscure nodal disease in the supraclavicular fossa and mediastinum respectively.

CT angiography and examination of the liver and pancreas is preferably performed using bolus-tracking technique (see below). When this is not available, the approximate examination start for CT angiography is 15–25 s, the late arterial phase (also called the portal-venous inflow phase) 25–30 s and the venous phase (also called portal, or portal-venous phase) 60–90 s after CM injection start. CT angiography may be needed in the preoperative setting, but usually the examination in the late arterial phase is sufficient to evaluate the anatomy of the arteries and their relation to the tumors. Also, the late arterial phase is in most cases sufficient for pNET diagnosis, and examination in the so-called pancreatic phase (at approximately 40 s after CM injection start), which is advocated for CT of ductal pancreatic carcinoma, is generally not as advantageous for pancreatic neuroendocrine tumor (pNET) imaging.

For proper examination of the liver, a sufficient amount of iodine, optimally 0.75mg per kg body weight, needs to be injected in order to achieve adequate enhancement of the normal liver in the venous contrast-enhancement phase to optimise delineation of the poorly vascularised metastases. A high CM injection rate, at least 5 ml/s, results in proper enhancement of the aorta and the larger arteries for CT angiography. A similarly high i.v. CM influx is needed for enhancement of well-vascularised liver metastases in the late arterial phase and to achieve adequate enhancement of the pancreas and renal parenchyma. Importantly, a high CM injection rate allows a better separation over time between the various contrast-enhancement phases.

When the thorax and/or the neck is examined together with the abdomen, the amount of CM and the injection rates are adjusted compared to what is required to perform a proper CT of the abdomen. When the thorax and/or the neck, by contrast, are examined separately, the amount of CM injected and the injection rate can be decreased. MDCT of the neck also requires a somewhat lower CM injection rate: approximately 1.5–2 ml/kg body weight of CM 300–350 mg/ml is recommended to be injected at 2.5 ml/s and using a 40-s scanning delay. For CT examination of the thorax, even less CM and a lower injection rate can be used. Approximately 1–1.5 ml/kg body weight of CM 300–350 mg/ml is administered at about 1.5 ml/s and a scanning delay of 60 s is preferable.

For CT of the liver, a so-called triple-phase examination is required. This involves examination before (non-enhanced, native) and during i.v. contrast-enhancement in the late arterial (portal-venous inflow) phase and in the venous phase. For follow-up of NET liver metastases, some centers restrict CT examination to the venous contrast-enhancement phase and only when the initial imaging work-up has shown better delineation of the liver metastases in the non-enhanced examination and/or in the late arterial phase one or both of these phases are added. This routine is, however, insufficient since there is a risk that new well-vascularized metastases may escape detection. Also, fatty infiltration of the liver, which may be induced by medical therapy, can significantly change the imaging prerequisites. Liver metastases initially diagnosed during the venous phase may no longer be visible at follow-up, but show up in the non-enhanced examination and/or the late arterial contrast-enhancement phase. A triple-phase CT examination also reduces the risk of misinterpreting areas of normal parenchyma as metastases in a fatty infiltrated liver. In order to decrease the radiation dose to the patient, the possibility of using dual energy CT to produce virtual pre-contrast images can be considered.

Coordination of CT scanning in relation to the CM injection is best controlled by using the 'bolus-tracking' technique, for which computer software is regularly supplied together with the CT scanner. This allows for monitoring of the aortic enhancement during contrast medium administration in order to determine the optimum time point for the examination start. Various routines also exist in the use of the bolus-tracking technique. For CT angiography and examination in the late arterial phase a fixed attenuation value (around 150 Hounsfield units, HU) in the abdominal aorta may be used to initiate the scanning start. As an alternative, a lower value (around 100 HU) may be used to trigger the examination start but needs to be followed by a 10–15-s scan delay. In combined CT examinations of the abdomen and thorax, including triple-phase CT of the liver, the order that scanning of these body regions is performed depends on how the bolus-tracking technique is applied. Initially non-enhanced scanning of the liver is generally performed. Then the liver is examined in the late arterial phase and thereafter the thorax and abdomen in the venous phase. Alternatively, an examination of the thorax early after CM injection start is favored and coordinated so that the subsequent scanning of the liver is performed in the late arterial phase, and thereafter the whole abdomen is examined in the venous phase.

As discussed above, for CT enteroclysis, a naso-jejunal tube can be placed under fluoroscopy guidance downstream to the Treitz ligament. Unless already confirmed by fluoroscopy, pre-contrast CT examination is performed to check the correct position of the tube. Approximately, 2000 ml of warmed tap water is administered through the tube, preferably by using a pump at 150–200 ml/min. Intravenous glucagon or anticholinergic drug is recommended and CT during i.v. contrast-enhancement is performed 50 s after injection of 120–150 ml at 3 ml/s. Because small tumors are anticipated, reconstruction of thin, approximately 2 mm, sections are recommended and viewing using MPRs and cine-loop is mandatory.

Radiation Dose

The radiation dose administered to the patient varies with the examination protocol and the type of CT scanner. A high tube voltage, a high tube current, a long tube rotation time and a low pitch increase the dose. In order to maintain a proper image quality in large-size patients, the tube current is increased but it may be decreased in small size patients. This results in a higher radiation dose to large- compared to small-size patients. Automated radiation dose modulation software is currently routinely supplied with the CT scanner, whereby the tube current is adjusted automatically along the scan length depending on the body size (low in neck and higher in abdomen) and tissue composition (low in thorax and higher in the abdomen). Recently automated modulation of the tube potential (kV) has been introduced in some CT scanners to reduce the radiation dose to the patient. However, it should be noted that inaccurate diagnosis poses a signifant risk to patients and efforts to reduce radiation exposure should never lead to suboptimal imaging protocols.

An examination in a MDCT scanner ≤1 mm slice thickness (‘one run’) of a patient of 70 kg results in an approximate radiation dose of 6 mSv for the whole abdomen and 4 mSv for the upper abdomen (liver) from the diaphragm to the iliac crest. An optimal MDCT examination of the abdomen comprising three-phase CT of the liver and examination of the pelvis in this 70-kg patient thus results in a 14 mSv radiation dose. Corresponding figures for MDCT of the thorax is 3.5 mSv and of the neck is 4.5 mSv. The radiation dose the patient decreases with the use of modern automated radiation dose modulation software (mA and kV).

Image Findings

Gastric, duodenal, rectal and colonic NETs are often diagnosed by endoscopy and EUS. The role of CT when the primary site is already confirmed is to detect regional and distant metastases for staging of the disease.

For type 1 and type 2 gastric NETs, CT is not required except for large (>2 cm) and invasive tumors detected by EUS. Type 1 tumors are predominantly located in the fundus and body of the stomach and are typically multicentric, <1 cm in diameter, rounded with sharp margin and contrast-enhancing. Type 2 gastric NETs are usually multiple and located within the stomach wall, which is thickened secondary to gastrin hypersecretion due to a gastrinoma present in the pancreas or duodenum as a part of the MEN-1 or Zollinger-Ellison syndrome. Type 3 gastric NETs are solitary, large lesions, with a more irregular and more diffusely delineated margin that may ulcerate. These tumors can also extend into the peri-gastric fat.

Duodenal NETs are usually small contrast-enhancing tumors and in the case of gastrinomas, as part of MEN I syndrome, may be multiple. For CT diagnosis of the primary tumor it is important to distend the duodenum with water and to perform the examination during i.v. contrast-enhancement since this will facilitate detection of the usually markedly contrast-enhancing tumor which is depicted against the low attenuating water in the bowel lumen (Figure 1).

Functional pNETs, such as insulinoma, and incidental non-functioning pNETs are typically small and sharply delineated. They can be multiple in patients with the MEN-1 syndrome. These tumors tend to be best visualised as evenly contrast-enhancing tumors in the portal-venous inflow phase (at approximately 30s) rather than in the pancreatic
contrast-enhancement phase (at approximately 40s after CM injection start) (Figure 2). In the venous contrast-enhancement phase, pNETs usually exhibit higher attenuation than the surrounding normal pancreas.

Other functional pNETs (solitary gastrinoma, VIPoma, glucagonoma) and non-functioning pNETs are usually larger (Figure 3) and may have calcifications that are best depicted in the non-contrast-enhanced examination. Larger pNETs may be well or not so well vascularised and often comprise areas of necrosis and the contrast-enhancement usually shows an irregular pattern. CT also

delineates the position of the tumor in relation to the pancreatic and common bile duct, evaluates possible vascular encasement (Figure 4) and stages the disease with respect to regional lymph node involvement and presence of distant metastases, mainly to the liver. With a usually slow-growing pNET occluding the pancreatic duct, this is dilated proximal to the occlusion and the surrounding pancreatic parenchyma is severely atrophic and appears like a thin brim surrounding the dilated duct. A large pNET can occasionally be confused with a cystadenoma or a ductal pancreatic cancer. An intrapancreatic accessory spleen in the tail may be misdiagnosed as a small pNET.

The small intestinal NETs (SI-NETs) may be diagnosed by endoscopy including capsule endoscopy and by CT-enteroclyis. In some centers MRI-enteroclysis is performed. SI-NETs are mostly found in the ileum rather than in the jejunum and are usually small and occasionally multiple. Consequently, these small tumors are difficult to diagnose as filling defects at CT with positive oral CM. With the use of a positive oral CM (e.g. diluted iodine or barium sulphate solution) the usually high attenuating SI-NET is more likely to escape detection than when the lesion is surrounded by a low attenuating CM such as water, similarly to what was previously discussed regarding diagnosis of duodenal tumors.

Frequently, SI-NETs present due to associated mesenteric metastases. These can induce an intense desmoplastic reaction causing contraction and tethering of the adjacent bowel loop resulting in partial or complete intestinal obstruction. Vascular encasement of the superior mesenteric artery and vein may compromise bowel circulation. At CT, this is reflected as an irregular soft tissue mass, typically with one or more areas of calcifications (Figure 5), surrounded by radiating streaks in the mesenteric fat (Figure 5) resembling spokes in a wheel. The superior mesenteric artery and/or vein or branches/tributaries of these vessels may be encased by the tumor. In this situation, surgical resection of the primary tumour and associated mesenteric lymph nodes can lead to vascular compromise of the small bowel, leading to short-bowel syndrome if recognized intra-operatively, or ischemic complications in the post-operative period if not. A preoperative imaging report should therefore include a description of the number of arterial branches from the superior mesenteric artery and tributaries to the superior mesenteric vein, respectively, above the mesenteric metastasis. A classification of mesenteric lymph nodes into five stages according to their proximity to the trunk and/or branches of the superior mesenteric artery has also been proposed to facilitate the surgical management [23].

For NETs of the colon and the rectum, the role of CT is not to detect the primary tumor or to appreciate its invasion of the rectal wall and the surrounding mesorectum, which is usually performed better by MRI or EUS. Colonic NETs are generally diagnosed by colonoscopy and fluoroscopy, and CT is therefore utilised to stage rectal and colonic NETs by detecting regional and distant metastases and, in case of locally advanced tumors, to visualise infiltration into adjacent organs and tissues.

CT cannot definitively differentiate liver metastases due to NETs from any other malignant tumors. Typically, NET liver metastases are well vascularised and best depicted during i.v. contrast-enhancement in the late arterial phase where they show up as high attenuating (bright) lesions in the non-enhanced (dark) normal liver (Figure 6). However, poorly vascularized NET liver metastases are also frequent. These are best depicted in the venous contrast-enhancement phase as low attenuating (dark) areas relative to the normal contrast-enhanced high attenuating (bright) liver parenchyma (Figure 7). Larger metastases are fairly often visible in the pre-contrast images in which occasional areas of calcification are best seen. Peripheral contrast enhancement and central necrosis in larger NET liver metastases are often seen. In the pre-contrast examination NET liver metastases are generally low attenuating relative to the normal liver.

Viewing of the CT examination should always be performed using window settings optimised for image reading of soft tissues, lung and bone, sequentially. For liver and pancreas it may be necessary to adjust the window setting and decrease the window width and to increase the window center (level) in the contrast-enhanced images to optimize lesion detection.

The CT appearance of NET lymph node metastases is similar to those from other malignant tumors, although a marked contrast enhancement may be seen. However, some particular anatomical sites should be kept in mind during image reading. In addition to the mesentery and the retroperitoneum, lymph node metastases from SI-NETs can often be found ventrally in the lower thorax adjacent to the thoracic wall and to the heart (Figure 8), in the mediastinum and supraclavicular. Also, retrocrural lymph node metastases are not infrequent (Figure 9). When evaluating the CT examination for lymph node metastases, in anatomical regions where these may be surrounded by fat, it is often helpful to

adjust the window setting by increasing the window width to facilitate lesion detection. Also, the use of MPRs is advantageous for depiction of small lymph node metastases. Peritoneal carcinomatosis is fairly frequent and, most often found in the ventral aspect of the abdomen as irregular web like bands and/or as nodular lesions (Figure 9). Ovarian metastases are occasionally found (Figure 10).
NET bone metastases are often sclerotic (blastic), (Figure 11) but can be osteolytic and sometimes show a mixed appearance. Breast metastases from SI-NETs are not infrequent and are generally to the ductal tissue rather than to fatty tissue and can therefore be mistaken for primary breast carcinoma. Brain metastases are fairly rare but can be diagnosed at contrast-enhanced CT, generally as rounded contrast-enhancing (bright) lesions. Lung metastases from NETs are fairly rare and, similarly to those from other malignant tumors, appear as rounded, usually multiple and generally well-delineated soft tissue opacities, predominantly in the lower lobes.

Documentation and Reporting of Results

For research, the RECIST 1.0 (Response Evaluation Criteria in Solid Tumours) and in recent years also RECIST 1.1 [24] are regularly used as the reference standard by which tumor response to treatment is reported and these criteria are therefore advantageous when comparing the results of different trials. Measurable lesions should exceed 1 cm largest diameter. Necrotic or confluent lesions should not be measured. Bone metastases, pleural fluid, ascites, peritoneal carcinomatosis and leptomeningeal disease also represent non-measurable lesions. New lesions should be reported and except for the quantitative description of the measurable lesion sizes and the sum of lengths, also a qualitative description of the tumors regarding treatment response, e.g. necrosis, should be reported. One of the important updates in RECIST 1.1 is that the short-axis of lymph nodes ≥1.5 cm is measured. The contrast-enhancement phase in which the lesions are best depicted should be reported. In order to accurately communicate the diagnostic information, liaison between radiologists and clinicians is essential.
In clinical trials, in the case of liver metastases, the liver tumor burden is sometimes also separately reported as the proportion of total liver volume, for example < 10%, 10-25%, 25-50%, > 50%. This adds important prognostic information and can influence decisions regarding debulking surgery and locoablative therapies. There are several manual and computer software based methods to facilitate the quantification of liver tumor load at CT. These methods generally rely on sufficient difference in

attenuation /contrast-enhancement between the metastases and the normal liver, respectively, and some patients are therefore difficult to assess. These methods are still investigational.

Magnetic Resonance Imaging

For imaging of the abdomen, bone and brain, MRI is generally better than CT and is therefore preferred if available, although it may also be complimentary to CT. The image contrast in MRI is generally better with MRI than CT and the use of a number of MRI sequences facilitates tissue characterization and hence diagnosis. The use of hepatocyte-specific CM makes MRI advantageous compared to CT for liver imaging. Because MRI does not expose the patient to radiation, the uptake and excretion of iv CM may be effectively imaged at multiple time points by repeated acquisitions (dynamic MRI). However, due to its restricted availability in many centers, MRI was previously mainly used as a problem-solving tool when CT failed. This has changed over the last few years and MRI is more frequently applied as first line imaging.

Hard- and Software Requirements

The currently available scanners have high field-strengths, generally between 1.5 T and 3.0 T. The use of a phased-array torso coil is recommended and thin sections (3 mm and not more than 5 mm) are preferable. The image quality for various MRI sequences may vary between vendors and they need to be set up in close collaboration with the vendor engineer and the MRI physicist, technologist and radiologist at the MRI unit. Fast acquisitions in 3D during one breath hold are recommended during i.v. contrast-enhancement to decrease respiratory image artifacts. The use of fat-suppressed sequences is recommended to increase the tissue contrast. For MRI of the pancreas, MR cholangiopancreatography (MRCP, at least 2D coronal radiated thick slices sequences) is advantageous to visualize the pancreatic duct.

Diffusion-weighted imaging (DWI) is an MRI technique that is receiving much attention in oncology [25] and utilizes a regular phased-array torso coil. Based on the restriction of water molecule movement, mainly due to a narrowing of the intercellular space, DWI offers high lesion-to-background contrast for tumor imaging, including NETs. No contrast administration is needed to obtain DW-MRI.

Dynamic contrast enhanced MRI (DCE-MRI) and perfusion imaging are non-invasive methods to examine microvascular structure and function, by tracking the pharmacokinetics of injected low-molecular weight, usually gadolinium-based, contrast agents as they pass through the tumor vasculature. Quantitative DCE techniques enable the calculation of combined physiological processes e.g. blood flow, blood volume, and vessel permeability. These quantitative techniques are still investigational for assessment of response to antiangiogenic therapies [26,27].

Sensitivity, Specificity and Detection Rates

The MRI reports on sensitivity and specificity for NET are few, and variations regarding MRI acquisition protocols between studies make it difficult to compare and compile literature data on imaging efficacy. Older studies, utilizing a few classical sequences such as transverse T1 and T2 without contrast-enhancement, generally shows lower imaging yield [28-29] than in recent reports in which the type of i.v. CM may vary, i.e. hepatocyte-specific versus extracellular CM [11,30-37].
MRI including diffusion-weighted imaging (DWI), which will be described below, yield additional tumor findings [38-39] but comparisons between DWI-MRI studies are hampered by the use of different sets of b-values.
Mean and range diagnostic accuracy results based on the number of patients and studies for NETs are presented in Table 2 [11,28-34,40-43].

Patient Information and Preparation

The presence of certain magnetic metal implants and pacemakers is considered a contraindication for performing MRI, with some being relative and others absolute contraindications. Patients should be asked about any previous metal implant procedures so that the material can be checked against a list of implants, available at MRI departments, that precludes an MRI examination. These contraindications are even more important with 3T systems and one must choose a lower field magnet when appropriate.
Claustrophobia is more pronounced with MRI than CT and the patient should be informed that during the examination he or she will be placed in a long tunnel and will have to remain still during the approximately 30-minute examination. If the patient is claustrophobic, administration of an anxiolytic agent may be necessary. During the examination, the patient should be provided with ear protection against the sound of the scanner, although newer scanners have “quiet” sequences. When CM needs

to be administered i.v. access is obtained and before some examinations, e.g. of the small bowel, the patient needs to be at the department an hour in advance of imaging to achieve filling of the bowel. Before MRI of the pancreas, the patient must be fasting for 6 hours. Shortly before starting the examination, distension of the stomach and duodenum with paramagnetic agent such as frozen/thawed blueberries or pineapple juice, is advantageous to decrease image artefacts related with water that may impair the image quality, especially of MRCP.

The patient's history should be checked for diabetes and renal impairment and pregnancy. The risk for nephrogenic systemic fibrosis, which may be associated with the use of gadolinium-based CM in patients with chronic renal failure, should be assessed. The creatinine clearance should be calculated when Gd-contrast-enhancement is considered, and injection should not be performed if GFR< 30 ml/min. Intravenous Gd-based CM is avoided if at all possible in pregnant patients and the patient should be consented if there is a very strong indication to give it.

Examination Technique

The field of view should be kept as small as possible in order to optimize image quality. I.v. administration of an anti-peristaltic drug, e.g. butylscopolamine 20 mg or glucagon 1 mg (if butylscopolamine is not available) is recomended to optimise MRI of the abdomen. Short breath-hold or repiratory-triggered sequences are recommended when 'moving targets' such as liver, pancreas and bowel are examined.

The field of view and sequences chosen thus depend on the imaging needs. Some recommendations are provided as follows:

1. **Anatomical/morphological sequences:**
   Transverse T2 (either respiratory-gated or breath-hold for upper abdominal regions) with additional coronal T2 (for upper abdomen) and sagittal T2 (for lower abdomen/pelvis). Fat saturation of the T2 weighted images is an additional option (such as spectral inversion recovery, SPIR). Transverse T1, without and with fat saturation and out-of-phase (the Dixon technique is advised, which will provide in-phase, out-of-phase, water-only and fat-only images).

2. **Diffusion-weighted imaging:**

Diffusion-weighted MRI (DW-MRI) is based on the diffusion of water molecules that may be restricted by cell membranes. In hyper-cellular tissues, such as tumors, this is consequently reflected at MRI by a signal decrease in the apparent diffusion coefficient (ADC) images. DW-MRI is now routinely used for all abdominal studies. The acquisitions are performed using different so called b-values in the range 0-1000 s/mm^2 out of which usually three are chosen, typically one low (*b*0 or 50), one intermediate (e.g. *b*400) and one high (e.g. *b*600, 800 or 1000). Although DWI primarily provides information about tumor cell density, the low-b-value images also depict the anatomy quite well and offer better image quality, fewer artefacts and better sensitivity for lesion detection than fat-suppressed T2-weighted imaging [34].

A high b-value DWI provides better image contrast, minimizing the perfusion effect and yielding greater tissue diffusivity and a lower T_2 shine-through effect. For DWI-MRI of the pancreas b800 or b1000 are usually applied and b600 is the minimum for liver imaging. The ADC map derived from these data is used to confirm whether high signal intensity on the high b value image represents restricted diffusion (which would be low on the ADC map) or whether there is a T2-shine through effect (which would be high on the ADC map).

Ideally, the diffusion-weighted images are acquired such that they are anatomically matched to the conventional T1 and T2 weighted images in order to cross-correlate any findings. The final choice of b values to be used is not fully established. However, for qualitative assessment, the use of a low b value (e.g. 0 or 50) and a high b value (e.g. 800) with accompanying ADC map is sufficient for analysis of the presence or absence of restricted diffusion in a lesion.

3. Dynamic contrast enhancement:

Transverse dynamic Gd contrast-enhanced MRI is suitable for almost all body parts (except some bone examinations) with acquisition at 30, 70 and 120 seconds and at 3–5 minutes after injection start. 3D acquisitions are recommended and allow for reconstruction in various anatomical planes; typically transverse, coronal and sagittal images. The conventional extracellular Gd-based CM for MRI, with a pharmacokinetic pattern similar to

that of iodine CM used for CT, remains the standard for i.v. contrast-enhanced MRI. Hepatocyte-specific i.v. CM for characterization of liver lesions is optional but increasingly used. Gd-DTPA or Gd-EOB-DTPA immediately after injection act as extracellular contrast agents but are not eliminated with glomerular filtration. Instead they accumulate in the hepatocytes during a relatively long period of time following injection (approximately 15–120 min depending on the chelate) and thereby make tumor tissue appear hypointense in relation to the normal liver. They can help distinguish focal liver lesions of hepatocellular origin from lesions of non-hepatocellular origin (metastases), and can also be used in the evaluation of the biliary tree.

4. **Additional sequences for pancreatic evaluation:**

MRCP is mandatory to optimally evaluate the regional anatomy and the relation of the tumor to the pancreatic duct and the main bile duct. Coronal radiated T2 -weighted thick-slice (25 mm) sequences with two ranges including the pancreatobiliary junction (6 slices) and the pancreatic body (3 slices), respectively, is recommended; a 3D sequence may be added.

5. **Specific protocol for small bowel evaluation:**

The small bowel is initially distended with a large volume of fluid such as mannitol. Large field of view axial and coronal images are acquired including T2, T1 without and with fat saturation and T1 with fat saturation post Gd-contrast. The use of this technique depends on local expertise. The detection of small bowel NETs may initially undertake using capsule endoscopy.

6. **Whole-body MRI**

The acquisition protocol in WB-MRI constitutes a compromise between examination time and image detail. Whole-body MRI (WB-MRI) examination protocols encompassing the neck-thorax-abdomen (and brain when needed), with acquisition of DWI and i.v. contrast-enhanced images of the liver and pancreas, which are recommended, can now be performed in a total study time of 1h or less. While image quality of WB-MRI has increased considerably, for the sake of examination time, the number of acquisition

sequences needs to be reduced and typically results in lower spatial resolution than for an examination of a limited part of the body. A few studies reporting on WB-MRI on NETs have been published [42,43] and also together with PET in PET/MRI hybrid scanners [44-45]. The use of WB-MRI including DWI is increasing, also for NET imaging.

Image Findings

At MRI, a typical NET appears as a low signal intensity (dark) lesion in T1 - and an intermediate to high signal intensity (bright) lesion in T2 -weighted images (Figure 12a & b). The MRI appearances of NETs are similar to those of CT concerning tumor delineation, contrast-enhancement characteristics and various morphologic patterns (Figure 12c). Although spatial resolution is frequently poorer with MRI than CT, the much better soft tissue contrast of MRI facilitates the detection of small NETs.

pNETs

Detection of small pNETs is favorable with MRI (Figure 12 and 13), particularly with T_1 water selected and T_2 SPIR thin slices. PNETs are not typically associated with main pancreatic duct stenosis and upstream dilatation at MRCP. Concerning vascular behavior of NET, the most vascularised NETs have the lowest malignant potential and the best prognosis [46-48] (Figure 13). A benign pNET typically has a round or oval shape, is small (<2 cm) and hypervascular, and shows higher ADC values and ADC ratios than more aggressive pNETs (figures 1 and 2). A correlation between the ADC and tumor grade has been shown (Table 3) [49-50]. The image patterns of unequivocally malignant lesions are quite different [51].

Solid-appearing serous cystic neoplasms, intra-pancreatic accessory spleen and pancreatic metastasis may be considered as differential diagnoses when imaging appearances suggest a pNET. Similar to pNETs, the majority of solid-appearing serous cystic neoplasms appear hypervascular on imaging. However, the latter differ significantly on MR showing high signal intensity and cystic component on T_2-weighted images. All serous cystadenomas show a non-restrictive pattern on the ADC map, while NETs show diffusion restriction [52].

A second differential diagnosis is an intra-pancreatic accessory spleen in the pancreatic tail. Typically, the signal intensity of the intra-pancreatic accessory spleen varies between MRI sequences in parallel with that of the spleen. Compared with the spleen, the accessory spleen has been shown to be iso-

intense more frequently than small pNETs on T_2-weighted images, arterial, portal and late phase images and DWI [53]. The ADC is usually lower in an accessory spleen than in a pNET [54]. A third differential diagnosis is an intrapancreatic metastasis from an unrelated (e.g. renal) cancer [55].

Liver metastases

Depiction of small liver metastases on MRI is facilitated by using multiple sequences including DW-MRI and dynamic i.v. contrast-enhancement [16,40,41] (Figures 14 and15). Lesions that are equivocal or contradictory at CT and US may better be characterized by MRI (Figure 15). NET liver metastases generally show high signal intensity on T_2 -weighted images. The contrast-enhancement kinetics on MRI obtained with extra-cellular Gd-based CM are similar to those with iodine-based CM for CT. Hypervascular metastases thus regularly (60-70 %) show heterogeneous intense Gd-contrast-enhancement in the hepatic arterial dominant-phase [40,56,57]. Ring-enhancement is a frequent (72% of 165 patients) finding in the hepatic arterial dominant phase [58] (Figure 15).

Hypovascular metastases are best depicted in the venous phase, similar to CT and appear as low-signal intensity lesions relative to the high-signal intensity contrast-enhancing normal liver parenchyma. Perilesional enhancement is frequent in the venous phase (92% of patients) and a peripheral low signal intensity area may be observed in the post-contrast late phase [58].

The high signal intensity of NET liver metastases on T_2 -weighted images make their distinction from cavernous haemangioma difficult. However, these are generally easily identified based on their typical contrast-enhancement pattern (similar to that on CT). Thus, in the arterial dominant contrast-enhancement phase a haemangioma typically displays globular peripheral skip enhancement. The contrast-enhancement will over time gradually extend towards the lesion center and fill the entire lesion making the haemangioma appear hyperintense in the venous and late phase. A liver metastasis will, by contrast, in this phase appear hypointense relative to the normal liver because of the CM washout from from the metastasis, or isointense. Furthermore, the haemangioma will not show restricted diffusion, and consequently has high ADC values, in contrast to the restricted diffusion and low ADC in a metastasis [56] .

Depiction of pathological lymph nodes

Because normal lymph nodes are of high cellularity it is difficult to apply DW-MRI to detect metastatic lymph nodes. There are no specific data concerning the diagnostic performance of MRI in detecting

NET nodal metastases. The application of MRI for locoregional staging of rectal NETs is mentioned in the CT section of this paper

Peritoneal carcinomatosis

Peritoneal carcinomatosis is challenging to image, particularly on CT, as there are frequently multiple but small volume sites of disease which are challenging to identify against the adjacent soft tissues, such as the bowel serosa. MRI may be helpful in problem solving if CT is equivocal, with both DWI and gadolinium-enhanced MRI being useful for depicting peritoneal metastases of small volume [42,43,59].

Therapy monitoring

Imaging assessment of therapy response by CT/MRI utilise RECIST, based on one-dimensional lesion measurements. There is, however, an increasing demand for evaluating other parameters than tumor size in order to earlier assess the treatment effect of the current generally costly NET therapies, many of which result in stabilization rather than tumor shrinkage. Dynamic contrast-enhanced MRI [26,27] and DWI [60] are currently being investigated in this respect.

Documentation and Reporting of Results

The documentation and reporting of results of MRI is similar to that of CT.

Templates for standardised reports and examination protocols are published as additional data on line.

Ultrasound

Sensitivity, Specificity and Detection Rates

Ultrasound (US) is known to be an operator-sensitive modality leading to wide variation regarding sensitivity and specificity of the reported series. The US-, Endoscopic US (EUS), intraoperative US, (IOUS) and contrast-enhanced US (CEUS) acquired sensitivity, specificity and detection rate (mean and range based on the number of patients and studies) for NETs at various anatomical sites is presented in Table 3.

For pNET diagnosis, a mean 39% (range 17–79%) detection rate was found in 6 studies on abdominal US including 153 patients [61-66].

EUS is the most sensitive method for diagnosing pNETs, showing a mean 86% (range 82-93%) sensitivity and 92% (range 86-95%) specificity in 3 studies comprising 149 patients [67-69]. The detection rate was 86% (range 75-97%) in 9 studies comprising 220 patients [9,62,63,66,70-74]. IOUS is also a sensitive method for detecting pNETs with a mean 92% (range 74–96%) detection rate reported in 4 studies that included 127 patients [64,66,75,76]. When insulinomas were considered separately, the mean detection rate of EUS was 86%
(range 57–100%) in 12 studies including 250 patients [63,64,72,77-85] and that of IOUS was, 92% (range 84–100%) in 9 studies on 264 patients [66,75,76,86-91]. For duodenal tumors and lymph node metastases, the detection rate of US was 18% in a study of 25 patients [66] and that of EUS 63% in 2 studies comprising 59 patients [66,72]

Studies reporting on US for the detection of liver metastases exclusively from NETs are scarce. However, in one study including 131 patients with various NETs, US exhibited 88% sensitivity and 95% specificity [12]. CEUS has been shown to be more sensitive for the diagnosis and characterization of liver lesions than conventional US. In 48 patients with NETs and suspicion of liver metastases, the sensitivity of CEUS was 82% [92]. The diagnostic yield of US-guided biopsies in 129 patients was shown to improve by CEUS compared to conventional US [93]. Liver haemangiomas were easier to characterize by CEUS than by pre-contrast US [94].

Hard- and Software Requirements

The possibility of using different transducers with appropriate ultrasound frequencies is important. The deeper portions of the abdomen require better penetration of a low-frequency transducer than more superficial areas where a high frequency transducer is preferred. With the recent development of US transducer, the frequency in one single transducer may be adjusted according to the different needs during the examination. By harmonic imaging technique the sensitivity of US can be improved. The use of i.v. CM for US is an important development of the technique, and preferably the US equipment software should allow for CEUS.

Patient Information and Preparation

The patient needs to be informed that the examination generally lasts 15–30 min, unless CEUS, which lasts longer, is performed. During US of the abdomen patients may repeatedly need to hold their breath for a few seconds and the insertion of an i.v. catheter before CEUS may cause some discomfort.

Information Provided by the Clinician

US of the abdomen in obese patients is difficult to perform and tends to be unreliable as abdominal organs cannot be sufficiently penetrated. These patients are better candidates for CT or MRI. An exception from this rule is US-guided biopsy, which can always be tried and, converted into a CT-guided procedure if necessary. The referring physician needs to provide information regarding the patient's diagnosis, kind of medical therapy, previous surgery, type of surgery and the findings at surgery and results of previous imaging examinations.

If CEUS is contemplated, information should be provided regarding previous insertion of cardiac valve prosthesis since the use of i.v. CM for US in these patients presently is not accurate (bubbles are broken by such prosthesis), and recent cardiac angina is a contraindication due to the risk of acute cardiac insufficiency. Please see also pertinent parts in the corresponding paragraph regarding CT and MRI.

Examination Technique

As opposed to CT, which allows fast and detailed examination of the whole abdomen and of additional body regions (thorax, neck) at the same session, US is better suited for examination of limited parts of the abdomen, for example the pancreas and the liver. Although time-consuming, examination of the whole abdomen is still feasible, although an overview of the tumor load in patients with extensive disease may be difficult.

Because US is an operator-dependent procedure, an optimal examination technique is essential. The use of different transducer frequencies is important. Low frequencies (about ≤3 MHz) better penetrates tissues, but high frequencies (approx. >5 MHz) allow for higher spatial resolution. The advantage and drawback of the high and low frequencies must be considered during the examination

and used accordingly for examination of deep and superficial parts of the abdominal organs, respectively.

Abdominal organs are generally easier to examine during a breath hold, and it is often advantageous to place the patient in different positions on the examination couch and perform US while the patient is standing up or during a Valsalva manoeuvre. This can be especially helpful for the examination of the pancreas, when bowel gas, especially in the transverse colon, prevents accurate ultrasound penetration.

Doppler techniques (power Doppler, colour-coded Doppler) are valuable in order to evaluate the tumor vascularity and are helpful in distinguishing vascular from non-vascular tubular structures.

By dynamic CEUS the temporal and spatial pattern of tumor uptake and washout (in- and outflow) of the CM may be evaluated. CEUS may therefore be considered for localisation of NET liver metastases and pNETs. By CEUS, liver metastases in the 2- to 3-mm range may be readily detected and previously equivocal tumor findings at unenhanced US, or CT, may be characterised. CEUS is mandatory when percutaneous radiofrequency ablation of liver metastases is considered. A limitation of the technique, however, is that the whole liver cannot be evaluated by US during all phases of contrast enhancement.

In case of negative preoperative US in patients with the Zollinger-Ellison syndrome, peroperative US is recommended by which the duodenal wall and pancreatic head can be explored.

Image Findings

Abdominal ultrasound and CT are complementary radiological methods used to diagnose pNET, liver metastases, lymph node and mesenteric metastases and US is an excellent tool for guiding the biopsy needle to obtain a tumor tissue specimen. By US, the bile ducts, the pancreatic duct and vessels may be evaluated for dilatation and tumor invasion and free fluid in the abdomen and pleural spaces may be detected. Intestinal tumors are rarely detected but are occasionally seen as a low echogenic wall thickening or polypoid

tumor, which is well vascularised. A large locally advanced intestinal NET infiltrating the surrounding tissues is more easily detected. The ability of US to differentiate an adenocarcinoma of the colon from a NET is poor.

A pNET is typically a low echogenic and hypervascular lesion. As with CT and MRI, the local extent of the tumor should be assessed. The relation of the pNET to the pancreatic duct and the common bile duct should be determined as well as any encasement or invasion of the splenic vein and the superior mesenteric artery and vein.

Mesenteric metastases from a SI-NET and mesenteric and retroperitoneal lymph node metastases are seen as low echogenic masses. The desmoplastic reaction, which by CT and MRI is a characteristic feature of a mesenteric metastasis from a SI-NET, cannot be detected by US.

NET liver metastases cannot be differentiated from any other type of liver metastases. Small (<1 cm) metastases generally appear as low echogenic rounded lesions, whereas large (>1 cm) metastases usually are highly echogenic with a low echogenic halo and may have central low echogenic necrosis. These lesions often appear hypervascular by Doppler techniques and CEUS. In patients with fatty infiltration of the liver, resulting in a high echogenic normal parenchyma, the NET metastases may instead appear low echogenic.

Documentation and Reporting of Results

The documentation and reporting of results by US is similar to that of CT and MRI. However, for therapy monitoring, the reported lesion sizes by US are generally difficult to compare with those measured by CT and MRI. This is because the size of the lesions, according to RECIST is measured regularly in the transaxial CT and MRI images. By US these tumors are instead measured in undefined anatomical imaging planes, usually the one in which the lesions appears largest. Also, it is generally difficult to assess the overall tumor load in patients with extensive disease by US. For example, tumor assessment in a patient in whom the normal liver is almost entirely replaced by metastases is generally unreliable by US. Therefore, US is not employed for initial diagnosis or therapy monitoring in clinical trials (except to evaluate superficial tumor lesions as an adjunct to estimating the lesion size by palpation). However, in the clinical setting, US is an excellent method for

diagnosis and characterisation of NETs. Since CT and US are complementary imaging methods, they may be used advantageously as alternating modalities for therapy monitoring in order to decrease the radiation dose to the patient, particularly to those who are young and have a long life expectancy.

Nuclear Medicine & Hybrid Imaging

Somatostatin receptor imaging

The value of somatostatin receptor imaging to assess the somatostatin receptor status of the patients tumors is twofold: firstly, somatostatin receptor scintigraphy (SRS) and, even more so, PET/CT using ^{68}Ga-labeled somatostatin analogs (i.e. 68Ga-DOTA-TOC/TATE/NOC), generally reveal several additional metastases compared to conventional radiological methods (CT/MRI) [6,96,97]. Secondly, demonstration of sufficient somatostatin receptor expression in the tumors makes the patient eligible for peptide receptor radiotherapy (PRRT).

Somatostatin is a regulatory peptide widely distributed in the human body, particularly in the central and peripheral nervous system, in the endocrine glands, in the immune system and in the gastrointestinal tract. In all these tissues, somatostatin action is mediated through membrane-bound receptors, of which five subclasses have been cloned (sst1–sst5) [96]. They all belong to the family of G-protein-coupled receptors. Only sst2, sst5 and, to some extent, sst3 have a high affinity for the commercially available synthetic octapeptide octreotide [99]. Somatostatin receptors are expressed in several normal human tissues, including brain, pituitary, gastrointestinal tract, pancreas, thyroid, spleen, kidney, immune cells, vessels and peripheral nervous system [100-103].
Somatostatin receptors have been identified *in-vitro* in a large number of human neoplasias. A high incidence and density of somatostatin receptors are found particularly in gatroenteropancreatic NETs, broncho-pulmonary carcinoids, pituitary adenoma, pheochromocytoma, paraganglioma, neuroblastoma, medullary thyroid cancer and small cell lung carcinoma [104]. Tumors of the nervous system including meningioma and medulloblastoma also very often express a high density of somatostatin receptors. Additionally, tumors not known to classically originate from endocrine or neural cells, such as lymphoma, breast cancer, renal cell cancer, hepatocellular cancer, prostate cancer, sarcoma and gastric cancer can express somatostatin receptors. In the majority of these tumors, the sst2 receptor subtype is predominantly expressed both when studied with receptor autoradiography or at the gene expression level, although low amounts of other somatostatin receptor

subtypes may be concomitantly present [105,106]. The expression of somatostatin receptors is not a tumor-specific characteristic and selected non-tumoral lesions may express somatostatin receptors for instance, active granulomas in sarcoidosis and inflamed joints in active rheumatoid arthritis [107]. With increasing proliferation (Ki-67) cellular somatostatin receptor expression generally decreases and consequently, so does tumor uptake on somatostatin receptor imaging [108,109]. The situation is usually the reverse for metabolic imaging by ^{18}FDG-PET/CT with lesions generally becoming more ^{18}FDG avid with increasing proliferation. For visualization of higher grade NETs, and especially neuroendocrine cancers (NECs), ^{18}FDG-PET/CT may therefore be preferred if lesion detection is required. Studies on patients undergoing both somatostatin receptor imaging and ^{18}FDG-PET/CT show the methods to be complementary and increase the sensitivity [109,110]. Because of financial restraints, this optimal dual nuclear imaging strategy is applied only in a few centers.

Interestingly, recent studies have shown that some of the low grade NETs also are ^{18}FDG avid and, consequently tumor uptake of ^{18}FDG has been shown of value to predict prognosis [111,112].

The mainstay for somatostatin receptor imaging has for long been SRS using ^{111}In-pentetreotide (Octreoscan™). However, PET/CT with ^{68}Ga-labeled somatostatin analogs (^{68}Ga-SSA) has replaced SRS as the method of choice in an increasing number of centers because of greater diagnostic accuracy and lower radiation dose. ^{68}Ga-SSA-PET/CT also offers better patient convenience since imaging may be performed 60 minutes after injection compared to SRS, which is performed 24h after injection of ^{111}In-pentetreotide. Additionally, image acquisition times are shorter, increasing patient comfort. Imaging after injection of ^{99m}Tc-labeled somatostatin analogs may similarly be performed the same day [113] but the preparation has limited availability in many European countries.

Apart from visualizing the somatostatin receptors, nuclear medicine procedures allows for *in-vivo* imaging of other biological processes, some of which have been proposed for NETs [114]. One of these clinically available tracers for PET/CT is ^{18}F-DOPA. This agent has been reported to provide high image quality and to be superior to Octreoscan and FDG-PET/CT, especially for SI-NETs [115]. However, ^{18}F-DOPA-PET/CT does not provide information on receptor expression and there are some practical disadvantages compared to ^{68}Ga-SSA-PET/CT, such as high cost and higher radiation dose to the patient. Also, in head-to-head comparisons with ^{68}Ga-SSA-PET/CT fewer tumors were detected by PET/CT with ^{18}F-DOPA than with ^{68}Ga-SSA although the patient-based results were similar [116,117]. For insulinoma, particularly the benign variant with often low somatostatin receptor

expression, agents that bind to the glugagon-like peptide receptor-1 (GLP-1) have recently been shown to be highly sensitive [118].

Sensitivity, Specificity and Detection Rates

According to recent studies the sensitivity of ^{111}In-pentetreotide scintigraphy (including SPECT) for NET detection in general is 60%-80% [97,119,120] and the specificity 92-100% [119-122]. Imaging results of SRS for various NET subtypes are listed in Table 4.

NET imaging results of PET/CT with different ^{68}Ga-DOTA-SSAs show small variations in comparative trials [123,124]. Four recent meta-analyses, with overlapping studies, on PET and PET/CT with ^{68}Ga-DOTA-SSAs have for NET detection shown mean sensitivities and specificities ranging 88-93% and 88-95%, respectively, detailed in Table 5 [125-128]. As discussed above, ^{18}FDG is generally better taken up in high grade than in low grade NETs and the imaging yield therefore depends on the ratios of NETs with respective tumor grades within the examined patient group. The sensitivity of ^{18}FDG-PET/CT for NET detection ranges 37-72% [109-111,129,130].

Hard- and Software Requirements

A gamma camera usually utilizes two sets of gamma detectors in front of and behind the patient, respectivel. **The detectors are moved along the patient, stepwise or through a very slow continuous motion, to acquire** planar images (anterior and posterior views). Additionally, the detectors are rotated stepwise around the patient to produce single photon emission computed tomography (SPECT) images. **Usually SPECT includes either the abdomen or the thorax, but sometimes both, depending on the imaging needs and hardware features.** Recent gamma cameras also include a CT unit by which a fully diagnostic CT may be performed (SPECT/CT). The introduction of SPECT/CT has increased the diagnostic yield and the readers´ confidence, similarly to that shown for PET/CT compared to stand alone PET, and is **therefore** recommended. SRS is generally performed 24h after ^{111}In-pentetreotide injection and includes planar imaging (anterior and posterior views) and SPECT/CT. Early acquisition at 4h post injection may also be performed but has been abandoned in many departments due to the resulting inconvenience for patients and because it seldom obviates the need for delayed imaging. Similarly, 48h images were previously acquired in order not to confuse bowel radioactivity with tumor lesions, but with **SPECT/CT** hybrid imaging,this is only rarely necessary. SPECT images are generally reconstructed also as MIP volumes and MPRs in

the transversal, coronal and sagittal planes. **With** hybrid scanners, SPECT/CT overlays (fusion images) are generally also produced in the transversal, coronal and sagittal planes.

The PET/CT scanner resembles a CT scanner with a bed for the patient but with a longer tunnel (gantry). Usually the CT unit is placed in the front and the detector rings in the posterior part of the gantry. The examination generally starts with a CT overview ("scout view") with the X-ray tube in a fixed position in the gantry to produce a frontal and sometimes also a lateral view. On this/these overviews the respective fields of views for the CT and PET examinations are indicated. **Because of the 15-20 cm detector ring coverage the bed of the scanner is moved stepwise through the gantry and the PET acquisition is performed 2-3 minutes per "bed position" to generally include from the proximal thighs to the base of the scull.**

In general, PET/CT is performed using a protocol comprising a scanogram/scout view/topogram, a low-dose CT for attenuation correction (CT-AC) and a standard diagnostic CT examination during i.v. contrast-enhancement**, CT is acquired** while the patient continues tidal breathing, because deep inspiration will **result in** misregistration with PET and may introduce unacceptable artifacts. When a diagnostic CT is not warranted the CT-AC is optimally performed with a **somewhat higher** radiation dose to enable anatomical correlation of the PET findings **(apart for attenuation correction).** This CT can provide the non-contrast component of a subsequent contrast-enhanced study focussed on the pancreas or liver as indicated the clinical setting and findings on PET. When performed as a stand-alone investigation, acquisition of a fully diagnostic CT is preferred unless contraindicated (kidney impairment, intolerance to contrast medium) or recently **performed** (last 3-4 weeks). Thus, for CT in the framework of PET/CT and SPECT/CT, similar protocols as for stand-alone diagnostic CT are preferred (please see CT section), applying scan parameters to minimize patient radiation exposure. The diagnostic i.v. contrast-enhanced CT is regularly not used for attenuation correction because high intravascular (and sometimes intestinal) concentrations of CM may cause artefacts in the reconstructed PET images following CT-attenuation correction and, acceptable thus, affect quantification and should therefore follow PET acquisition. Some centers, however, consider that CT in the venous phase is acceptable for attenuation correction and refrain from a separate CT-AC [131]. The PET/CT images are regularly reconstructed in the transverse, coronal and sagittal planes and also as PET/CT fusion images in these planes. Image reading requires a computer software that

generally is supplied by the gamma camera or PET/CT vendor. Some of these computer softwares include functions to handle transverse SPECT, PET and CT image volumes and display them as MPRs and SPECT/CT and PET/CT fusions, respectively, and do not require previous image preparation at the scanner. Similar functions are incorporated in some PACS workstation software.

Patient Information, Preparation and Precautions

The question of either stopping or continuing somatostatin analog medication before somatostatin receptor imaging is currently under debate. There are published data showing increased tumor uptake and decreased normal tissue uptake of ^{68}Ga-DOTATOC by i.v. injection of octreotide in connection with PET/CT [132]. The quality of ^{68}GaDOTATOC-PET/CT was also found to be unaffected by somatostatin analog medication before the examination [133]. There is therefore no need to stop short-acting somatostatin analog medication if required for symptom control. However, in patients receiving long-acting preparations, somatostatin receptor imaging should be scheduled shortly before the next injection. If needed, the patient may switch to a short-acting somatostatin analog during this interval.

To reduce radiation exposure, patients should be well hydrated before and for at least 1 day after injection. A mild oral laxative is adviced before SRS, especially when the abdomen is the area of interest, and may be administered the evening before ^{111}In-pentetreotide injection and the evening after injection. Laxatives are not required before PET/CT and usually not when SPECT/CT is available. There is no need for fasting prior to somatostatin receptor imaging, but before ^{18}FDG-PET/CT at least 4h and optimally 6h fasting period is recommended. The feasibility of the **examination procedure** in patients on hemodialysis (with imaging after dialysis) should be discussed with local nephrologists and radiation protection experts.

Precautions needs to be taken in patients suspected of having insulinoma, for whom an i.v. infusion of glucose should be available because of the potential for inducing severe hypoglycemia. Neither ^{111}In-pentetreotide nor PET tracers should be injected into central i.v. lines or together with solutions for total parenteral nutrition. The usual precautions and considerations for nuclear medicine investigations in pregnant or breastfeeding women apply.

Information Provided by the Clinician

A relevant history of the type of suspected or known primary tumor, its hormonal activity, the results of other imaging studies (CT or MRI), laboratory results (tumor markers), history of recent surgery,

chemo- therapy, radiation therapy, and somatostatin analog therapy should be obtained. In the case of a hybrid (SPECT/CT, PET/CT) examination, information on the patient´s kidney function (serum-creatinine) and history of previous contrast medium related adverse events is required.

Examination Technique and Image Acquisition

The recommended administered activity of ^{111}In-pentetreotide (OctreoScan™) is 185–222 MBq (5–6 mCi) in adults and 5 MBq/kg (0.14 mCi/kg) in children. The amount of pentetreotide injected is 10–20 µg and is not expected to have a clinically significant pharmacological effect. Before the administration of ^{111}In-pentetreotide, the labeling yield of the radiopharmaceutical should be tested according to the manufacturer's instructions. The radiopharmaceutical should be used within 6 h of preparation.

Planar scintigraphy images are acquired using a large-field-of-view gamma camera fitted with a medium-energy collimator. Symmetrical 20% energy windows are centered over both photopeaks of ^{111}In (173 and 247 keV) and the data from both windows are added. Planar localized images of the head, chest, abdomen, pelvis, and, if needed, the extremities can be acquired for 10–15 min/image. For whole-body images using a dual-head camera, acquisition should be for a minimum of 30 min (head to upper femurs) and longer for the entire body (e.g., a speed of up to 3 cm/min has been suggested) in a single pass. Since cervical lymph node metastases may be missed on the whole-body images, additional planar localized images of the head and neck, including lateral views, are suggested unless SPECT/CT is available.

SPECT/CT imaging of the appropriate regions, as indicated based on the clinical history, should be per formed preferably with a multi-detector gamma camera 24h after injection. Although imaging systems may vary, an example of potentially useful acquisition parameters for a multi-detector system are the following: 3° angular sampling, 128 x128 matrix, 360° rotation, 20–30 s/stop. The SPECT/CT acquisition usually takes approximately 35-45 minutes and about twice this time when both abdomen and thorax are included.

^{68}Ga-DOTA-TOC/TATE/NOC is administered i.v. (approximately 2MBq/kg BW) as a bolus and PET/CT examination is performed 60 minutes after injection. The highest NET uptake of ^{68}Ga-DOTATOC was registered approximately 70 min post injection [6] which indicates that the optimal

imaging time point is approximately 60 minutes post injection when allowing for a compromise between lesion uptake and statistical quality, which decreases fairly rapidly due to the short half-life of ^{68}Ga. Logistic issues posed by this short half-life has led some departments to use a 30-minute uptake interval in order to increase the patient throughput from each tracer synthesis.

Approximately 4 MBq/kg body weight of ^{18}FDG is administered as a bolus and PET/CT is performed after 60 minutes. This activity may vary in case of obese patients or in anticipation of delayed imaging. Blood glucose level must be measured prior to administering ^{18}FDG. Although efforts should be made to decrease blood glucose to **a physiological** level, hyperglycaemia should not represent an absolute contraindication for performing the study [131]. In particular, for clinical studies: If plasma glucose level is <11 mmol/L (or ≤200 mg/dL) the ^{18}FDG-PET/CT study can be performed.

If plasma glucose level is ≥11 mmol/L (or >200 mg/dL) the ^{18}FDG-PET/CT study should be rescheduled. The following recommendations apply to patients with diabetes mellitus:

• Type II diabetes mellitus (controlled by oral medication)

-The ^{18}FDG-PET/CT study should preferably be performed in the late morning.

-Patients must comply with the fasting rules indicated above.

-Patients continue to take oral medication to control their blood sugar. Metformin should be discontinued at the time of the procedure and withheld for 48 hours subsequent to the procedure if intravenous contrast is administered.

• Type I diabetes mellitus and insulin-dependent type II diabetes mellitus: Ideally, an attempt should be made to achieve normal blood-glucose values prior to ^{18}FDG-PET/CT, in consultation with the patient and his/her attending medical doctor. There are three options for scheduling the ^{18}FDG-PET/CT study:

(1) It can be scheduled for late morning or mid-day. In this case, the patient should eat a normal breakfast by early morning (around 7.00 a.m.) and inject the normal amount of insulin. Thereafter the patient should not consume any more food or fluids, apart from the prescribed amount of water.

(2) It can be scheduled for early morning. The presence of long acting insulin administered the evening before should not interfere with the ^{18}FDG-PET/CT study and blood-glucose will likely still be under control. The patient should eat a normal breakfast after the ^{18}FDG-PET/CT study and inject the normal amount of insulin.

(3) In the case of patients on continuous insulin infusion, if possible the ^{18}FDG-PET/CT study

should be scheduled early in the morning. The insulin pump is kept on the "night setting" until after the ^{18}FDG-PET/CT study. The patient can have breakfast after the ^{18}FDG-PET/CT study.

As previously stated, a diagnostic i.v. contrast-enhanced CT examination is recommended together with PET/CT and filling of the bowel is therefore started 1h before examination during which the patients drinks 800ml of tap water. Patients should void immediately before PET/CT. PET acquisition (both ^{68}Ga-DOTA-TOC/TATE/NOC and ^{18}FDG) is performed in 3D and generally includes from the base of the skull to the proximal thighs and 3 minutes acquisition per bed position. The PET/CT examination time is approximately 20 minutes including diagnostic i.v. contrast-enhanced CT using similar protocols as for stand alone CT.

Radiation Dose

^{111}In-pentetreotide is cleared rapidly from the blood. Excretion is almost entirely through the kidneys (50% of the injected dose is recovered in the urine by 6 h, 85% within 24 h). Hepatobiliary excretion is only about 2% of the administered dose. The effective dose is 0.054 mSv/MBq. For a full patient dose of 222 MBq this is 12 mSv.

^{68}Ga-DOTATOC-SSAs are excreted through the kidneys. The radiation dose from ^{68}Ga-DOTATOC/TATE to a 70 kg patient is approximately 2.9 mSv (effective dose for 68Ga-DOTATOC/TATE =0.021 mSv/MBq), [124,134]. The coefficient for effective dose from ^{18}FDG in adults is 0.019 mSv/MBq [135], i.e. about 3.5 mSv for an administered activity of 185 MBq. The radiation exposure related to CT, carried out as part of PET/CT or SPECT/CT, is with modern hybrid systems similar to that of stand-alone CT scanners (please see CT section). When a recent diagnostic CT/MRI already is available, a low radiation dose CT examination is sufficient for attenuation correction and anatomical correlation of the PET and SPECT findings, with an approximate 2 mSv effective dose.

Image Findings

Normal tissue distribution on somatostatin receptor imaging is found in the anterior pituitary, thyroid and spleen, due to receptor binding. Uptake in the kidneys is for the most part due to reabsorption of the radiolabeled peptide in the renal tubular cells after glomerular filtration. High activity concentrations are found in the urinary collective system and in the urinary bladder. The bowel is usually visualized to varying degrees. Hepatobiliary clearance of ^{111}In-petetreotid into the bowel also

occurs, necessitating the use of laxatives in order to facilitate the interpretation of abdominal images although, as pointed out previously, the regular use of SPECT has reduced this interpretation problem.

False-positive results of SRS have been reported. In virtually all cases the term 'false-positive' is a misnomer because somatostatin receptor-positive lesions that are not related to the pathology for which the investigation is performed, are present. Many of these have been reviewed by Gibril et al. [136]**.** The most common of these are listed in Table 6.

Accumulation of ^{68}Ga-DOTA-SSAs is similar to that of ^{111}In-pentetreotide but also with high physiological accumulation in the adrenal glands. Also, the uptake in the uncinate process of the pancreas may be very high in some patients, and is related to the high abundance of pancreatic polypeptide (PP) cells in this part of the pancreas [137]. This finding should not be mistaken for a pNET in which case morphological correlation of the tracer uptake at contrast-enhanced CT/MR is expected.

^{18}FDG is accumulates in the brain with a vey high uptake and is excreted by the kidneys with high radioactivity concentrations in kidney pelvices, ureters and urinary bladder. Physiological uptake is seen in the lymphoid tissue of the pharynx, larynx, and variably in the myocardium, stomach, segments of bowel, activated muscle and brown fat (both typically in the neck). ^{18}FDG is also accumulated in areas of inflammation and infection, for instance after surgery and external radiation therapy.

Interpretation Criteria and Reporting of Results

SRS should if available be performed by using hybrid imaging (SPECT/CT). Otherwise SRS evaluation needs to be performed in correlation with recent relevant anatomic images (CT/MRI). Knowledge of normal tissue accumulation patterns of ^{111}In-pentetreotide, ^{68}Ga-DOTA-SSAs and ^{18}FDG is important for study interpretation.

In the imaging report it is recommended to start with a procedure description stating the timing of imaging relative to radiopharmaceutical administration, areas imaged and for SRS whether SPECT was performed and, if so, its timing and body areas included.

Study limitations may sometimes be stated. For example some tumors may lack somatostatin receptors or the appropriate receptor subtypes and, therefore, escape detection, typically benign insulinomas. Small lesions detected at morphological imaging (CT/MRI) may not appear receptor positive because of the limited spatial resolution of the method (SPECT approximately 1.5 cm and PET about 0.5 cm). However, smaller lesions with high uptake may be detected, especially when located in tissues with low physiological tracer accumulation (high tumor-to-backgrund ratio). Functional image findings should be reported in correlation to those of the concomitantly performed CT, and vice versa.

Summary

CT constitutes the basic radiological method for primary NET diagnosis, staging, and surveillance after surgery and for therapy monitoring. CT is vastly available and provides fast and detailed contrast-enhanced imaging of extended body areas (neck-thorax-abdomen-pelvis). Because of inadequate morphological criteria (short axis measurements) characterization of lymph nodes by CT is difficult and bone metastases are often missed. CT imaging of pNET and metastases to the liver and brain is inferior to that of MRI.

Dynamic contrast-enhanced MRI of the liver and pancreas is therefore preferred, for example in the initial staging and for the preoperative imaging work-up. MRI is also preferred for imaging of metastases to brain and bone. MRI is less well suited for examination of extended body areas, because of the comparably longer examination procedure. Recent whole-body MRI protocols include dynamic contrast-enhanced examination of the liver and diffusion-weighted imaging but. In order not to exceed one-hour examination time, the image detail of the whole-body MRI is generally not as high as with dedicated MRI protocols for examination of more limited parts of the body. MRI may miss small lung metastases.

US frequently provides the initial diagnosis of liver metastases and contrast-enhanced US is an excellent method to characterize liver lesions that remain equivocal on CT/MRI.US is the method of choice to guide the biopsy needle for the histopathological NET diagnosis of abdominal lesions. US cannot visualize lesions in the thorax, brain or bone. CT guided biopsy is therefore used for NET lesions in the thorax and in bone. EUS is the most sensitive method to diagnose pancreatic NETs and also allows biopsy. Inraoperative US facilitates lesion detection/localization in the pancreas and liver.

Somatostatin receptor imaging by ^{68}Ga-DOTA-somatostatin analog-PET/CT provide high sensitivity for imaging of most types of NET lesions and should always be a part of the tumor staging, preoperative imaging and re-staging. SRS should be performed when PET/CT is not available but is considerably less sensitive. Bone metastases that are often missed on CT are much better visualized by ^{68}Ga-DOTA-somatostatin analog-PET/CT and lymph node metastases, that are not possible to characterize on CT/MRI, may be diagnosed. Visualization of mall peritoneal lesions and primary small-intestinal NETs is facilitated by ^{68}Ga-DOTA-somatostatin analog-PET/CT. ^{18}FDG is better suited for PET/CT of G3 and high G2 NETs, which generally have higher glucose metabolism and less SSTR expression than the low grade NETs. Findings of ^{18}FDG positive NETs at PET/CT indicate worse prognosis.

Conclusion

Accurate imaging of NETs is critical to management decisions and should always be tailored to answering relevant clinical questions. These may include suitability for surgery, choice of therapy, response to treatment or evaluation of symptoms. With a range of modalities that have both independent and complementary diagnostic roles, the imaging specialist should be aware of the strengths and limitations of each in order to be able to recommend the best test for the given clinical scenario. It should be recognized that sensitivity and specificity results provided in this article are subject to the intrinsic biases of the selection criteria used to enter patients into the study, the prevalence of disease in the population studied and the variable biology of NETs, which particularly influences the performance of molecular imaging techniques, which rely of expression of particularly cell characteristics. Whichever test is chosen, attention to detail in study acquisition and interpretation is vital to achieve the best possible outcomes. These guidelines are designed to help the imaging specialist in achieving these goals but may need to be adapted according to local availability, regulations and experience.

Other Antibes Consensus Conference participants

Bartsch, D.K. (Department of Surgery, Philipps University, Marburg, Germany), Borbath, I. (Service de Gastroenterologie, Cliniques Universitaires St-Luc, Bruxelles, Belgium), Capdevila, J. (Vall d'Hebron University Hospital, Teknon Institute of Oncology, Barcelona, Spain), Caplin, M. (Neuroendocrine Tumour Unit, Royal Free Hospital, London, UK), Chen, Y.-J. (Peking Union Medical College Hospital, Chinese Academy of Medical Sciences, Beijing, China), Costa, F. (Hospital Sírio Libanês, São Paulo, Brazil), Couvelard, A. (Service de Pathologie, Hôpital Bichat, Paris, France), Davies, P. (Neuroendocrine Tumour Unit, Royal Free Hospital,

London, United Kingdom), de Herder, W.W. (Department of Internal Medicine, Division of Endocrinology, ENETS Centre of Excellence Rotterdam, Erasmus MC, Rotterdam, the Netherlands), Delle Fave, G. (Department of Digestive and Liver Disease, Ospedale Sant'Andrea, Rome, Italy), Falkerby, J. (Deptartment of Endocrine Oncology, Uppsala University Hospital, Uppsala, Sweden), Ferone, D. (Department of Endocrine and Metabolic Sciences, University of Genoa, Genoa, Italy), Garcia-Carbonero, R. (Medical Oncology Department, Hospital Universitario Doce de Octubre, Madrid, Spain), Grozinsky-Glasberg S. (Neuroendocrine Tumor Unit, Endocrinology and Metabolism Service, Department of Medicine, Hadassah-Hebrew University Medical Center, Jerusalem, Israel), Gorbunova, V. (Department of Oncology, Institution of Russian Academy of Medical Sciences), Gross, D. (Department of Endocrinology & Metabolism, Hadassah University Hospital, Mevasseret Tsion, Israel), Grossman, A. (Oxford Centre for Diabetes, Endocrinology and Metabolism, Churchill Hospital, Oxford, United Kingdom), Hörsch, D. (Gastroenterology and Endocrinology Center for Neuroendocrine Tumors Bad Berka, Bad Berka, Germany), Tiensuu Janson, E. (Deptartment of Endocrine Oncology, Uppsala University Hospital, Uppsala, Sweden), Jensen, R.T. (Digestive Diseases Branch, NIH, Bethesda, Md., USA), Kaltsas, G. (Department of Pathophysiology, Division of Endocrinology, National University of Athens, Athens, Greece), Knigge, U. (Neuroendocrine Tumor Center of Excellence, Rigshospital, Copenhagen University Hospital, Copenhagen, Denmark), Kos-Kudla, B. (Department of Endocrinology, Medical University of Silesia, Katowice, Poland), Kulke, M.H. (Dana-Farber Cancer Institute, Harvard Medical School, Boston, Massachusetts, USA), Niederle, B. (Department of Surgery, Medical University of Vienna, Vienna, Austria), Nieveen van Dijkum, E.J.M. (Department of Surgery, Academic Medical Center, Amsterdam, the Netherlands), Öberg, K. (Department of Medical Sciences, Endocrine Oncology Unit, University Hospital, Uppsala, Sweden), Pape, U.-F. (Department of Hepatology and Gastroenterology, Campus Virchow Klinikum, Charité Universitätsmedizin Berlin, Berlin, Germany), Pascher, A. (Department of Surgery, Charité-Universitaetsmedizin Berlin, Berlin, Germany), Pavel, M. (Department of Hepatology and Gastroenterology, Campus Virchow Klinikum, Charité Universitätsmedizin Berlin, Berlin, Germany), Perren A. (Institute of Pathology, University of Bern, Switzerland), Ramage, J. (Gastroenterology Department, Hampshire Hospitals NHS Trust, Hampshire, United Kingdom), Reed, N. (Beatson Oncology Centre, Gartnavel General Hospital, Glasgow, United Kingdom), Rindi, G. (Institute of Anatomic Pathology, Policlinico A. Gemelli, Università Cattolica del Sacro Cuore, Rome, Italy), Rinke, A. (Division of Gastroenterology and Endocrinology, University Hospital Marburg (UKGM), Marburg, Germany), Ruszniewski, P. (Department of Gastroenterology, Beaujon Hospital, Clichy, France), Scoazec, J.-Y. (Services de pathologie morphologique et moléculaire, Département de biologie et pathologie médicales, Gustave Roussy Cancer Campus, Villejuif, France), Sorbye, H. (Dept. of Oncology, Haukeland University Hospital, Bergen, Norway), Toumpanakis, C. (Neuroendocrine Tumour Unit, Royal Free Hospital, London, United Kingdom), Welin, S. (Department of Medical Sciences, Endocrine Oncology, Uppsala University, Sweden).

References

1. Sundin A, Vullierme MP, Kaltsas G, Plöckinger U; Mallorca Consensus Conference participants; European Neuroendocrine Tumor Society. ENETS Consensus Guidelines for the Standards of Care in Neuroendocrine Tumors: radiological examinations. Neuroendocrinology. 2009;90(2):167-83

2. Kwekkeboom DJ, Krenning EP, Scheidhauer K, Lewington V, Lebtahi R, Grossman A, Vitek P, Sundin A, Plöckinger U; Mallorca Consensus Conference participants; European Neuroendocrine Tumor Society. ENETS Consensus Guidelines for the Standards of Care in Neuroendocrine Tumors: somatostatin receptor imaging with (111)In-pentetreotide. Neuroendocrinology. 2009;90(2):184-9

3. Koopmans KP, de Vries EG, Kema IP, Elsinga PH, Neels OC, Sluiter WJ, van der Horst-Schrivers AN, Jager PL. Staging of carcinoid tumours with 18F-DOPA PET: a prospective, diagnostic accuracy study. Lancet Oncol. 2006 Sep;7(9):728-34.

4. Ruf J, Schiefer J, Furth C, Kosiek O, Kropf S, Heuck F, Denecke T, Pavel M, Pascher A, Wiedenmann B, Amthauer H. 68Ga-DOTATOC PET/CT of neuroendocrine tumors: spotlight on the CT phases of a triple-phase protocol. J Nucl Med. 2011 May;52(5):697-704.

5. Veit-Haibach P, Schiesser M, Soyka J, Strobel K, Schaefer NG, Hesselmann R, Clavien PA, Hany TF. Clinical value of a combined multi-phase contrast enhanced DOPA-PET/CT in neuroendocrine tumours with emphasis on the diagnostic CT component. Eur Radiol. 2011 Feb;21(2):256-64

6. Gabriel M, Decristoforo C, Kendler D, Dobrozemsky G, Heute D, Uprimny C, Kovacs P, Von Guggenberg E, Bale R, Virgolini IJ. 68Ga-DOTA-Tyr3-octreotide PET in neuroendocrine tumors: comparison with somatostatin receptor scintigraphy and CT. J Nucl Med. 2007 Apr;48(4):508-18.
7. Fidler JL, Fletcher JG, Reading CC, Andrews JC, Thompson GB, Grant CS, Service FJ. Preoperative detection of pancreatic insulinomas on multiphasic helical CT. AJR Am J Roentgenol. 2003 Sep;181(3):775-80.
8.Ichikawa T, Peterson MS, Federle MP, Baron RL, Haradome H, Kawamori Y, Nawano S, Araki T. Islet cell tumor of the pancreas: biphasic CT versus MR imaging in tumor detection. Radiology. 2000 Jul;216(1):163-71.
9. Gouya H, Vignaux O, Augui J, Dousset B, Palazzo L, Louvel A, Chaussade S, Legmann P. CT, endoscopic sonography, and a combined protocol for preoperative evaluation of pancreatic insulinomas. AJR Am J Roentgenol. 2003 Oct;181(4):987-92.
10. Procacci C, Carbognin G, Accordini S, Biasiutti C, Bicego E, Romano L, Guarise A, Minniti S, Pagnotta N, Falconi M. Nonfunctioning endocrine tumors of the pancreas: possibilities of spiral CT characterization. Eur Radiol. 2001;11(7):1175-83.
11. Kitano M, Millo C, Rahbari R, Herscovitch P, Gesuwan K, Webb RC, Venkatesan AM, Phan GQ, Hughes MS, Libutti SK, Nilubol N, Linehan WM, Kebebew E. Comparison of 6-18F-fluoro-L-DOPA, 18F-2-deoxy-D-glucose, CT, and MRI in patients with pancreatic neuroendocrine neoplasms with von Hippel-Lindau disease. Surgery. 2011 Dec;150(6):1122-1128.
12. Chiti A, Fanti S, Savelli G, Romeo A, Bellanova B, Rodari M, van Graafeiland BJ, Monetti N, Bombardieri E. Comparison of somatostatin receptor imaging, computed tomography and ultrasound in the clinical management of neuroendocrine gastro-entero-pancreatic tumours. Eur J Nucl Med. 1998 Oct;25(10):1396-403.
13. Dahdaleh FS, Lorenzen A, Rajput M, Carr JC, Liao J, Menda Y, O'Dorisio TM, Howe JR. The value of preoperative imaging in small bowel neuroendocrine tumors. Ann Surg Oncol. 2013 Jun;20(6):1912-7
14. Kumbasar B, Kamel IR, Tekes A, Eng J, Fishman EK, Wahl RL. Imaging of neuroendocrine tumors: accuracy of helical CT versus SRS. Abdom Imaging. 2004 Nov-Dec;29(6):696-702
15. Hubalewska-Dydejczyk A, Fröss-Baron K, Mikołajczak R, Maecke HR, Huszno B, Pach D, Sowa-Staszczak A, Janota B, Szybiński P, Kulig J. 99mTc-EDDA/HYNIC-octreotate scintigraphy, an efficient method for the detection and staging of carcinoid tumours: results of 3 years' experience. Eur J Nucl Med Mol Imaging. 2006 Oct;33(10):1123-33.
16. Elias D, Lefevre JH, Duvillard P, Goéré D, Dromain C, Dumont F, Baudin E. Hepatic metastases from neuroendocrine tumors with a "thin slice" pathological examination: they are many more than you think... Ann Surg. 2010 Feb;251(2):307-10
17. Kim JH, Eun HW, Kim YJ, Lee JM, Han JK, Choi BI. Pancreatic neuroendocrine tumour (PNET): Staging accuracy of MDCT and its diagnostic performance for the differentiation of PNET with

uncommon CT findings from pancreatic adenocarcinoma. Eur Radiol. 2015 Aug 8. [Epub ahead of print]
18. Ambrosini V, Nanni C, Zompatori M, Campana D, Tomassetti P, Castellucci P, Allegri V, Rubello D, Montini G, Franchi R, Fanti S. (68)Ga-DOTA-NOC PET/CT in comparison with CT for the detection of bone metastasis in patients with neuroendocrine tumours. Eur J Nucl Med Mol Imaging. 2010 Apr;37(4):722-7
19. Putzer D, Gabriel M, Henninger B, Kendler D, Uprimny C, Dobrozemsky G, Decristoforo C, Bale RJ, Jaschke W, Virgolini IJ. Bone metastases in patients with neuroendocrine tumor: 68Ga-DOTA-Tyr3-octreotide PET in comparison to CT and bone scintigraphy. J Nucl Med. 2009 Aug;50(8):1214-21.
20. Johanssen S, Boivin M, Lochs H, Voderholzer W. The yield of wireless capsule endoscopy in the detection of neuroendocrine tumors in comparison with CT enteroclysis. Gastrointest Endosc. 2006 Apr;63(4):660-5.
21. Pilleul F, Penigaud M, Milot L, Saurin JC, Chayvialle JA, Valette PJ. Possible small-bowel neoplasms: contrast-enhanced and water-enhanced multidetector CT enteroclysis. Radiology. 2006 Dec;241(3):796-801.
22. ESUR guidelines on CM
23. Lardière-Deguelte S, de Mestier L, Appéré F, Vullierme MP, Zappa M, Hoeffel C, Noaves M, Brixi H, Hentic O, Ruszniewski P, Cadiot G, Panis Y, Kianmanesh R. Toward Preoperative Classification of Lymph-Node Metastases in Patients with Small Intestine Neuroendocrine Tumours in the Era of Intestinal-Sparing Surgery. Neuroendocrinology. 2015 Oct 8. [Epub ahead of print]
24. Eisenhauer EA, Therasse P, Bogaerts J, Schwartz LH, Sargent D, Ford R, Dancey J, Arbuck S, Gwyther S, Mooney M, Rubinstein L, Shankar L, Dodd L, Kaplan R, Lacombe D, Verweij J. New response evaluation criteria in solid tumours: revised RECIST guideline (version 1.1). Eur J Cancer. 2009 Jan;45(2):228-47.

25. Taouli B, Beer AJ, Chenevert T, Collins D, Lehman C, Matos C, Padhani AR, Rosenkrantz AB, Shukla-Dave A, Sigmund E, Tanenbaum L, Thoeny H, Thomassin-Naggara I, Barbieri S, Corcuera-Solano I, Orton M, Partridge SC, Koh DM. Diffusion-weighted imaging outside the brain: Consensus statement from an ISMRM-sponsored workshop. J Magn Reson Imaging. 2016 Feb 19. doi: 10.1002/jmri.25196. [Epub ahead of print]

26. de Mestier L, Dromain C, d'Assignies G, Scoazec JY, Lassau N, Lebtahi R, Brixi H, Mitry E, Guimbaud R, Courbon F, d'Herbomez M, Cadiot G. Evaluating digestive neuroendocrine tumor progression and therapeutic responses in the era of targeted therapies: state of the art. Endocr Relat Cancer. 2014 Apr 28;21(3):R105-20.

27. Miyazaki K, Orton MR, Davidson RL, d'Arcy JA, Lewington V, Koh TS, Thng CH, Leach MO, Collins DJ, Koh DM. Neuroendocrine tumor liver metastases: use of dynamic contrast-enhanced MR imaging to monitor and predict radiolabeled octreotide therapy response. Radiology. 2012 Apr;263(1):139-48.

28. Termanini B, Gibril F, Reynolds JC, Doppman JI, Chen CC, Stewart CA, Sutliff VE, Jensen RT: Value of Somatostatin Receptor Scintigraphy: A Prospective Study in Gastrinoma of its Effect on Clinical Management. Gastroenterology 1997:112,2:335 –347.

29. Carlson B, Johnson CD, Stephens DH, Ward EM, Kvols LK. MRI of pancreatic islet cell carcinoma. J Comput Assist Tomogr. 1993 Sep-Oct;17(5):735-40.

30. Caramella C, Dromain C, Baere T, Boulet B, Schlumberger M, DucreuxM E, Baudin E: Endocrine pancreatic tumours: which are the most useful MRI sequences? Eur Radiol 2010;20: 2618–2627GAS
31. Schmid-Tannwald C, Schmid-Tannwald CM, Morelli JN, Neumann R, Haug AR, Jansen N, Nikolaou K, Schramm N, Reiser MF, Rist C. Comparison of abdominal MRI with diffusion-weighted imaging to 68Ga-DOTATATE PET/CT in detection of neuroendocrine tumors of the pancreas. Eur J Nucl Med Mol Imaging. 2013 Jun;40(6):897-907
32. Thoeni RF, Mueller-Lisse UG, Chan R, Do NK, Shyn PB. Detection of small, functional islet cell tumors in the pancreas: selection of MR imaging sequences for optimal sensitivity. Radiology. 2000 Feb;214(2):483-90.
33. Brenner R, Metens T, Bali M, Demetter P, Matos C: Pancreatic neuroendocrine tumor: Added value of fusion of T2-weighted imaging and high b-value diffusion-weighted imaging for tumor detection. European Journal of Radiology 2012;81: 746– 749
34. Mayerhoefer ME, Ba-Ssalamah A, Weber M, Mitterhauser M, EidherrH, Wadsak W,Raderer M, Trattnig S,Herneth A, Karanikas G : Gadoxetate-enhanced versus diffusion-weighted MRI for fused Ga-68-DOTANOC PET/MRI in patients with neuroendocrine tumours of the upper abdomen. Eur Radiol 2013;23:1978-1985
35. Ceelen F, Theisen D, de Albéniz XG, Auernhammer CJ, Haug AR, D'Anastasi M, Paprottka PM, Rist C, Reiser MF, Sommer WH. Towards new response criteria in neuroendocrine tumors: which changes in MRI parameters are associated with longer progression-free survival after radioembolization of liver metastases? J Magn Reson Imaging. 2015 Feb;41(2):361-8.

36. Schreiter NF, Nogami M, SteffenI, Pape UF, Hamm B, Brenner W, Röttgen R. Evaluation of the potential of PET-MRI fusion for detection of liver metastases in patients with neuroendocrine tumours. Eur Radiol (2012) 22:458–467
37. Wulfert S, Kratochwil C, Choyke PL, Afshar-Oromieh A,Mier W, Kauczor HU, Schenk JP, Haberkorn U, Giesel1 FL. Multimodal Imaging for Early Functional Response Assessment ofof 90Y-/177Lu-DOTATOC Peptide Receptor Targeted Radiotherapy with DW-MRI and 68Ga-DOTATOC-PET/CTMol Imaging Biol 2014;16:586-594.
38. Moryoussef F, de Mestier L, Belkebir M, Deguelte-Lardière S, Brixi H, Kianmanesh R, Hoeffel C, Cadiot G. Impact on Management of Liver and Whole-Body Diffusion-Weighted Magnetic Resonance Imaging Sequences for Neuroendocrine Tumors: A Pilot Study. Neuroendocrinology. 2016 Apr 28. [Epub ahead of print]

39. De Robertis R, D"Onofrio M, Zamboni G, Tinazzi Martini P, Gobbo S, Capelli P, Butturini G, Girelli R, Ortolani S, Cingarlini S, Pederzoli P, Scarpa A. Pancreatic Neuroendocrine Neoplasms: Clinical Value of Diffusion-Weighted Imaging. Neuroendocrinology. 2015 Dec 9. [Epub ahead of print]

40. d'Assignies G, Fina P, Bruno O, Vullierme MP, Tubach F, Paradis V, Sauvanet A, Ruszniewski P, Vilgrain V. High sensitivity of diffusion-weighted MR imaging for the detection of liver metastases from neuroendocrine tumors: comparison with T2-weighted and dynamic gadolinium-enhanced MR imaging. Radiology. 2013 Aug;268(2):390-9.

41. Dromain C, de Baere T, Lumbroso J, Caillet H, Laplanche A, Boige V, Ducreux M, Duvillard P, Elias D, Schlumberger M, Sigal R, Baudin E. Detection of liver metastases from endocrine tumors: a prospective comparison of somatostatin receptor scintigraphy, computed tomography, and magnetic resonance imaging. J Clin Oncol. 2005 Jan 1;23(1):70-8.

42. Etchebehere EC, de Oliveira Santos A, Gumz B, Vicente A, Hoff PG, Corradi G, Ichiki WA, de Almeida Filho JG, Cantoni S, Camargo EE, Costa FP. 68Ga-DOTATATE PET/CT, 99mTc-HYNIC-octreotide SPECT/CT, and whole-body MR imaging in detection of neuroendocrine tumors: a prospective trial. J Nucl Med. 2014 Oct;55(10):1598-604

43. Schraml C, Schwenzer NF, Sperling O, Aschoff P, Lichy MP, Müller M, Brendle C, Werner MK, Claussen CD, Pfannenberg C. Staging of neuroendocrine tumours: comparison of [^{68}Ga]DOTATOC multiphase PET/CT and whole-body MRI. Cancer Imaging. 2013 Mar 5;13:63-72.

44. Hope TA, Pampaloni MH, Nakakura E, VanBrocklin H, Slater J, Jivan S, Aparici CM, Yee J, Bergsland E. Simultaneous (68)Ga-DOTA-TOC PET/MRI with gadoxetate disodium in patients with neuroendocrine tumor. Abdom Imaging. 2015 Aug;40(6):1432-40.

45. Beiderwellen KJ, Poeppel TD, Hartung-Knemeyer V, Buchbender C, Kuehl H, Bockisch A, Lauenstein TC. Simultaneous 68Ga-DOTATOC PET/MRI in patients with gastroenteropancreatic neuroendocrine tumors: initial results. Invest Radiol. 2013 May;48(5):273-9

46. Couvelard A, O'Toole D, Turley H, Leek R, Sauvanet A, Degott C, Ruszniewski P, Belghiti J, Harris AL, Gatter K et al.Microvascular density and hypoxia-inducible factor pathway in pancreatic endocrine tumours: negative correlation of microvascular density and VEGF expression with tumour progression. British Journal of Cancer 2005;92:94–101.

47. Rodallec M, Vilgrain V, Couvelard A, Rufat P, O'Toole D, Barrau V, Sauvanet A, Ruszniewski P & Menu Y. Endocrine pancreatic tumours and helical CT: contrast enhancement is correlated with microvascular density, histoprognostic factors and survival. Pancreatology 2006;6:77–85.

48. D'Assignies G, Couvelard A, Bahrami S, Vullierme M-P, Hammel P, Hentic O, Sauvanet A, Bedossa P, Ruszniewski P & Vilgrain V. Pancreatic endocrine tumors: tumor blood flow assessed with perfusion CT reflects angiogenesis and correlates with prognostic factors. Radiology 2009;250:407–416.

49. Jang KM, Kim SH, Lee SJ, Choi D. The value of gadoxetic acid-enhanced and diffusion-weighted MRI for prediction of grading of pancreatic neuroendocrine tumors. Acta Radiol. 2014 Mar;55(2):140-8

50. Wang Y, Zongming E, Chen ZE, Yaghmai V, Nikolaidis P, McCarthy RJ, Merrick L, Miller FH. Diffusion-Weighted MR Imaging in Pancreatic Endocrine Tumors Correlated With Histopathologic Characteristics. Journal of magnetic resonance imaging 33:1071–1079 (2011)
51. Manfredi R, Bonatti M, Mantovani W, Graziani R, Segala D,Capelli P,Butturini G, Pozzi Mucelli R: Non-hyperfunctioning neuroendocrine tumours of the pancreas: MR imaging appearance and correlation with their biological behaviour.Eur Radiol 2013;23:3029–3039
52. Park HS, Kim SY, Hong SM, Park SH, Lee SS, Byun JH, Kim JH, Kim HJ, Lee MG. Hypervascular solid-appearing serous cystic neoplasms of the pancreas: Differential diagnosis with neuroendocrine tumours. Eur Radiol. 2015 Sep 2. [Epub ahead of print]
53. Jang KM, Kim SH, Lee SJ, Park MJ, Lee MH, Choi D. Differentiation of an intrapancreatic accessory spleen from a small (<3-cm) solid pancreatic tumor: value of diffusion-weighted MR imaging. Radiology. 2013 Jan;266(1):159-67
54. Kang BK, Kim JH, Byun JH, Lee SS, Kim HJ, Kim SY, Lee MG. Diffusion-weighted MRI: usefulness for differentiating intrapancreatic accessory spleen and small hypervascular neuroendocrine tumor of the pancreas. Acta Radiol. 2014 Dec;55(10):1157-65

55. Moletta L, Milanetto AC, Vincenzi V, Alaggio R, Pedrazzoli S, Pasquali C. Pancreatic secondary lesions from renal cell carcinoma. World J Surg. 2014 Nov;38(11):3002-6.

56. Duran R, Ronot M, Kerbaol A, Van Beers B, Vilgrain V: Hepatic hemangiomas: factors associated with T2 shine-through effect on diffusion-weighted MR sequences. Eur J Radiol. 2014;83(3):468-78
57. Dromain C, de Baere T, Baudin E, Galline J, Ducreux M, Boige V, Duvillard P, Laplanche A, Caillet H, Lasser P, Schlumberger M, Sigal R. MR imaging of hepatic metastases caused by neuroendocrine tumors: comparing four techniques. AJR Am J Roentgenol. 2003 Jan;180(1):121-8.
58. Danet IM, Semelka RC, Leonardou P, Braga L, Vaidean G, Woosley JT, Kanematsu M. Spectrum of MRI appearances of untreated metastases of the liver. AJR Am J Roentgenol. 2003 Sep;181(3):809-17.
59. Li B, Li Q, Nie W, Liu S. Diagnostic value of whole-body diffusion-weighted magnetic resonance imaging for detection of primary and metastatic malignancies: A meta-analysis European Journal of Radiology 2014;83: 338– 344

60. Kukuk GM, Mürtz P, Träber F, Meyer C, Ullrich J, Gieseke J, Ahmadzadehfar H, Ezziddin S, Schild HH, Willinek WA. Diffusion-weighted imaging with acquisition of three b-values for response evaluation of neuroendocrine liver metastases undergoing selective internal radiotherapy. Eur Radiol. 2014 Feb;24(2):267-76.

61. Galiber AK, Reading CC, Charboneau JW, Sheedy PF 2nd, James EM, Gorman B, Grant CS, van Heerden JA, Telander RL. Localization of pancreatic insulinoma: comparison of pre- and intraoperative US with CT and angiography. Radiology. 1988 Feb;166(2):405-8.
62. Zimmer T, Ziegler K, Bäder M, Fett U, Hamm B, Riecken EO, Wiedenmann B. Localisation of neuroendocrine tumours of the upper gastrointestinal tract. Gut. 1994 Apr;35(4):471-5.

63. Zimmer T, Stölzel U, Bäder M, Koppenhagen K, Hamm B, Buhr H, Riecken EO, Wiedenmann B. Endoscopic ultrasonography and somatostatin receptor scintigraphy in the preoperative localisation of insulinomas and gastrinomas. Gut. 1996 Oct;39(4):562-8.
64. Pitre J, Soubrane O, Palazzo L, Chapuis Y. Endoscopic ultrasonography for the preoperative localization of insulinomas. Pancreas. 1996 Jul;13(1):55-60.
65. Angeli E, Vanzulli A, Castrucci M, Venturini M, Sironi S, Zerbi A, Di Carlo V, Pozza G, Del Maschio A. Value of abdominal sonography and MR imaging at 0.5 T in preoperative detection of pancreatic insulinoma: a comparison with dynamic CT and angiography. Abdom Imaging. 1997 May-Jun;22(3):295-303.
66. De Angelis C, Carucci P, Repici A, Rizzetto M. Endosonography in decision making and management of gastrointestinal endocrine tumors. Eur J Ultrasound. 1999 Nov;10(2-3):139-50.
67. Rösch T, Lightdale CJ, Botet JF, Boyce GA, Sivak MV Jr, Yasuda K, Heyder N, Palazzo L, Dancygier H, Schusdziarra V, et al. Localization of pancreatic endocrine tumors by endoscopic ultrasonography. N Engl J Med. 1992 Jun 25;326(26):1721-6.
68. Ardengh JC, de Paulo GA, Ferrari AP. EUS-guided FNA in the diagnosis of pancreatic neuroendocrine tumors before surgery. Gastrointest Endosc. 2004 Sep;60(3):378-84.
69. Anderson MA, Carpenter S, Thompson NW, Nostrant TT, Elta GH, Scheiman JM: Endoscopic ultrasound is highly accurate and directs management in patients with neuroendocrine tumors of the pancreas. Am J Gastroenterol 2000; 95: 2271–2277.
70. Glover JR, Shorvon PJ, Lees WR. Endoscopic ultrasound for localisation of islet cell tumours. Gut. 1992 Jan;33(1):108-10.
71. Zimmer T, Scherübl H, Faiss S, Stölzel U, Riecken EO, Wiedenmann B. Endoscopic ultrasonography of neuroendocrine tumours. Digestion. 2000;62 Suppl 1:45-50.
72. Proye C, Malvaux P, Pattou F, Filoche B, Godchaux JM, Maunoury V, Palazzo L, Huglo D, Lefebvre J, Paris JC: Noninvasive imaging of insulinomas and gastrinomas with endoscopic ultrasonography and somatostatin receptor scintigraphy. Surgery 1998; 124: 1134–1143.
73. Ruszniewski P, Amouyal P, Amouyal G, Grangé JD, Mignon M, Bouché O, Bernades P. Localization of gastrinomas by endoscopic ultrasonography in patients with Zollinger-Ellison syndrome. Surgery. 1995 Jun;117(6):629-35.
74. Fujimori N, Osoegawa T, Lee L, Tachibana Y, Aso A, Kubo H, Kawabe K, Igarashi H, Nakamura K, Oda Y, Ito T. Efficacy of endoscopic ultrasonography and endoscopic ultrasonography-guided fine-needle aspiration for the diagnosis and grading of pancreatic neuroendocrine tumors. Scand J Gastroenterol. 2016;51(2):245-52
75. Huai JC, Zhang W, Niu HO, Su ZX, McNamara JJ, Machi J. Localization and surgical treatment of pancreatic insulinomas guided by intraoperative ultrasound. Am J Surg. 1998 Jan;175(1):18-21.
76. Hiramoto JS, Feldstein VA, LaBerge JM, Norton JA. Intraoperative ultrasound and preoperative localization detects all occult insulinomas; discussion 1025-6. Arch Surg. 2001 Sep;136(9):1020-5.
77. Téllez-Ávila FI, Acosta-Villavicencio GY, Chan C, Hernández-Calleros J, Uscanga L, Valdovinos-Andraca F, Ramírez-Luna MÁ. Diagnostic yield of endoscopic ultrasound in patients with hypoglicemia and insulinoma suspected. Endosc Ultrasound. 2015 Jan-Mar;4(1):52-5.

78. Pongprasobchai S, Lertwattanarak R, Pausawasdi N, Prachayakul V. Diagnosis and localization of insulinoma in Thai patients: performance of endoscopic ultrasonography compared to computed tomography and magnetic resonance imaging. J Med Assoc Thai. 2013 Feb;96 Suppl 2:S187-93.
79. Joseph AJ, Kapoor N, Simon EG, Chacko A, Thomas EM, Eapen A, Abraham DT, Jacob PM, Paul T, Rajaratnam S, Thomas N. Endoscopic ultrasonography--a sensitive tool in the preoperative localization of insulinoma. Endocr Pract. 2013 Jul-Aug;19(4):602-8.
80. Varma V, Tariciotti L, Coldham C, Taniere P, Buckels JA, Bramhall SR. Preoperative localisation and surgical management of insulinoma: single centre experience. Dig Surg. 2011;28(1):63-73.
81. Nikfarjam M, Warshaw AL, Axelrod L, Deshpande V, Thayer SP, Ferrone CR, Fernández-del Castillo C. Improved contemporary surgical management of insulinomas: a 25-year experience at the Massachusetts General Hospital. Ann Surg. 2008 Jan;247(1):165-72.
82. Sotoudehmanesh R, Hedayat A, Shirazian N, Shahraeeni S, Ainechi S, Zeinali F, Kolahdoozan S. Endoscopic ultrasonography (EUS) in the localization of insulinoma. Endocrine. 2007 Jun;31(3):238-41.
83. Kaczirek K, Ba-Ssalamah A, Schima W, Niederle B. The importance of preoperative localisation procedures in organic hyperinsulinism--experience in 67 patients. Wien Klin Wochenschr. 2004 Jun 30;116(11-12):373-8.
84. Ardengh JC, Rosenbaum P, Ganc AJ, Goldenberg A, Lobo EJ, Malheiros CA, Rahal F, Ferrari AP. Role of EUS in the preoperative localization of insulinomas compared with spiral CT. Gastrointest Endosc. 2000 May;51(5):552-5.
85. Schumacher B, Lübke HJ, Frieling T, Strohmeyer G, Starke AA. Prospective study on the detection of insulinomas by endoscopic ultrasonography. Endoscopy. 1996 Mar;28(3):273-6.
86. Nakamura Y, Matsushita A, Katsuno A, Yamahatsu K, Sumiyoshi H, Mizuguchi Y, Uchida E. Clinical outcomes of 15 consecutive patients who underwent laparoscopic insulinoma resection: The usefulness of monitoring intraoperative blood insulin during laparoscopic pancreatectomy. Asian J Endosc Surg. 2015 Aug;8(3):303-9
87. Li W, An L, Liu R, Yao K, Hu M, Zhao G, Tang J, Lv F. Laparoscopic ultrasound enhances diagnosis and localization of insulinoma in pancreatic head and neck for laparoscopic surgery with satisfactory postsurgical outcomes. Ultrasound Med Biol. 2011 Jul;37(7):1017-23.
88. Nikfarjam M, Warshaw AL, Axelrod L, Deshpande V, Thayer SP, Ferrone CR, Fernández-del Castillo C. Improved contemporary surgical management of insulinomas: a 25-year experience at the Massachusetts General Hospital. Ann Surg. 2008 Jan;247(1):165-72.
89. Wong M, Isa SH, Zahiah M, Azmi KN. Intraoperative ultrasound with palpation is still superior to intra-arterial calcium stimulation test in localising insulinoma. World J Surg. 2007 Mar;31(3):586-92.
90. Chung JC, Choi SH, Jo SH, Heo JS, Choi DW, Kim YI. Localization and surgical treatment of the pancreatic insulinomas. ANZ J Surg. 2006 Dec;76(12):1051-5.
91. Grover AC, Skarulis M, Alexander HR, Pingpank JF, Javor ED, Chang R, Shawker T, Gorden P, Cochran C, Libutti SK. A prospective evaluation of laparoscopic exploration with intraoperative ultrasound as a technique for localizing sporadic insulinomas. Surgery. 2005 Dec;138(6):1003-8;
92. Mork H, Ignee A, Schuessler G, Ott M, Dietrich CF: Analysis of neuroendocrine tumour metastases in the liver using contrast-enhanced ultrasonography. Scand J Gastroenterol

2007; 42: 652–662.
93. Wu W, Chen MH, Yin SS, Yan K, Fan ZH, Yang W, Dai Y, Huo L, Li JY. The role of contrast-enhanced sonography of focal liver lesions before percutaneous biopsy. AJR Am J Roentgenol. 2006 Sep;187(3):752-61.
94. Bartolotta TV, Midiri M, Quaia E, Bertolotto M, Galia M, Cademartiri F, Lagalla R. Liver haemangiomas undetermined at grey-scale ultrasound: contrast-enhancement patterns with SonoVue and pulse-inversion US. Eur Radiol. 2005 Apr;15(4):685-93.
95. Srirajaskanthan R, Kayani I, Quigley AM, Soh J, Caplin ME, Bomanji J. The role of 68Ga-DOTATATE PET in patients with neuroendocrine tumors and negative or equivocal findings on 111In-DTPA-octreotide scintigraphy. J Nucl Med. 2010 Jun;51(6):875-82.
96. Frilling A, Sotiropoulos GC, Radtke A, Malago M, Bockisch A, Kuehl H, Li J, Broelsch CE. The impact of 68Ga-DOTATOC positron emission tomography/computed tomography on the multimodal management of patients with neuroendocrine tumors. Ann Surg. 2010 Nov;252(5):850-6.
97. Van Binnebeek S, Vanbilloen B, Baete K, Terwinghe C, Koole M, Mottaghy FM, Clement PM, Mortelmans L, Bogaerts K, Haustermans K, Nackaerts K, Van Cutsem E, Verslype C, Verbruggen A, Deroose CM. Comparison of diagnostic accuracy of ^{111}In-pentetreotide SPECT and ^{68}Ga-DOTATOC PET/CT: A lesion-by-lesion analysis in patients with metastatic neuroendocrine tumours. Eur Radiol. 2015 Jul 12. [Epub ahead of print]
98. Patel YC, Greenwood MT, Warszynska A, Panetta R, Srikant CB: All five cloned soma- tostatin receptors (hSSTR1–5) are function- ally coupled to adenylyl cyclase. Biochem Biophys Res Commun 1994;198:605–612.
99. Hoyer D, Epelbaum J, Feniuk W, et al: Soma- tostatin receptors; in Girdlestrom D (ed): The IUPHAR Compendium of Receptor Characterization and Classification. Lon- don, IUPHAR Media, 2000, pp 354–364.
100. Sreedharan SP, Kodama KT, Peterson KE, Goetzl EJ: Distinct subsets of somatostatin receptors on cultured human lymphocytes. J Biol Chem 1989;264:949–953.
101. Reubi JC, Horisberger U, Waser B, Gebbers JO, Laissue J: Preferential location of soma- tostatin receptors in germinal centers of hu- man gut lymphoid tissue. Gastroenterology 1992;103:1207–1214.
102. Reubi JC, Schaer JC, Markwalder R, Waser B, Horisberger U, Laissue JA: Distribution of somatostatin receptors in normal and neo- plastic human tissues: recent advances and potential relevance. Yale J Biol Med 1997;70: 471–479.
103. Csaba Z, Dournaud P: Cellular biology of so- matostatin receptors. Neuropeptides 2001; 35:1–23.
104. Reubi JC: Regulatory peptide receptors as molecular targets for cancer diagnosis and therapy. Q J Nucl Med 1997;41:63–70.
105. Reubi JC, Waser B, Schaer JC, Laissue JA: Somatostatin receptor sst1-sst5 expression in normal and neoplastic human tissues us- ing receptor autoradiography with subtype- selective ligands. Eur J Nucl Med 2001;28: 836–846.

106. Binderup T, Knigge U, Mellon Mogensen A, Palnaes Hansen C, Kjaer A. Quantitative gene expression of somatostatin receptors and noradrenaline transporter underlying scintigraphic results in patients with neuroendocrine tumors. Neuroendocrinology. 2008;87(4):223-32.

107. Reubi JC, Waser B, Krenning EP, Markusse HM, Vanhagen M, Laissue JA: Vascular somatostatin receptors in synovium from patients with rheumatoid arthritis. Eur J Phar- macol 1994;271:371–378.

108. Olsen IH, Langer SW, Federspiel BH, Oxbøl J, Loft A, Berthelsen AK, Mortensen J, Oturai P, Knigge U, Kjær A. (68)Ga-DOTATOC PET and gene expression profile in patients with neuroendocrine carcinomas: strong correlation between PET tracer uptake and gene expression of somatostatin receptor subtype 2. Am J Nucl Med Mol Imaging. 2016 Jan 28;6(1):59-72

109. Binderup T, Knigge U, Loft A, Mortensen J, Pfeifer A, Federspiel B, Hansen CP, Højgaard L, Kjaer A. Functional imaging of neuroendocrine tumors: a head-to-head comparison of somatostatin receptor scintigraphy, 123I-MIBG scintigraphy, and 18F-FDG PET. J Nucl Med. 2010 May;51(5):704-12.

110. Has Simsek D, Kuyumcu S, Turkmen C, Sanlı Y, Aykan F, Unal S, Adalet I. Can complementary 68Ga-DOTATATE and 18F-FDG PET/CT establish the missing link between histopathology and therapeutic approach in gastroenteropancreatic neuroendocrine tumors? J Nucl Med. 2014 Nov;55(11):1811-7.

111. Bahri H, Laurence L, Edeline J, Leghzali H, Devillers A, Raoul JL, Cuggia M, Mesbah H, Clement B, Boucher E, Garin E. High prognostic value of 18F-FDG PET for metastatic gastroenteropancreatic neuroendocrine tumors: a long-term evaluation. J Nucl Med. 2014 Nov;55(11):1786-90

112. Binderup T, Knigge U, Loft A, Federspiel B, Kjaer A. 18F-fluorodeoxyglucose positron emission tomography predicts survival of patients with neuroendocrine tumors. Clin Cancer Res. 2010 Feb 1;16(3):978-85

113. Cwikla JB, Mikolajczak R, Pawlak D, Buscombe JR, Nasierowska-Guttmejer A, Bator A, Maecke HR, Walecki J. Initial direct comparison of 99mTc-TOC and 99mTc-TATE in identifying sites of disease in patients with proven GEP NETs. J Nucl Med. 2008 Jul;49(7):1060-5

114. Koopmans KP, Neels ON, Kema IP, Elsinga PH, Links TP, de Vries EG, Jager PL. Molecular imaging in neuroendocrine tumors: molecular uptake mechanisms and clinical results. Crit Rev Oncol Hematol. 2009;71:199-213.

115. Balogova S, Talbot JN, Nataf V, Michaud L, Huchet V, Kerrou K, Montravers F. 18F-fluorodihydroxyphenylalanine vs other radiopharmaceuticals for imaging neuroendocrine tumours according to their type. Eur J Nucl Med Mol Imaging. 2013 ;40:943-66

116. Ambrosini V, Tomassetti P, Castellucci P, Campana D, Montini G, Rubello D, Nanni C, Rizzello A, Franchi R, Fanti S. Comparison between 68Ga-DOTA-NOC and 18F-DOPA PET for the detection of gastro-entero-pancreatic and lung neuro-endocrine tumours. Eur J Nucl Med Mol Imaging. 2008 ;35:1431-8.

117. Putzer D, Gabriel M, Kendler D, Henninger B, Knoflach M, Kroiss A, Vonguggenberg E, Warwitz B, Virgolini IJ. Comparison of (68)Ga-DOTA-Tyr(3)-octreotide and (18)F-fluoro-L-dihydroxyphenylalanine positron emission tomography in neuroendocrine tumor patients. Q J Nucl Med Mol Imaging. 2010 Feb;54(1):68-75.

118. Luo Y, Pan Q, Yao S, Yu M, Wu W, Xue H, Kiesewetter DO, Zhu Z, Li F, Zhao Y, Chen X. Glucagon-Like Peptide-1 Receptor PET/CT with 68Ga-NOTA-Exendin-4 for Detecting Localized Insulinoma: A Prospective Cohort Study. J Nucl Med. 2016 ;57(5):715-20.

119 (118. Sainz-Esteban A, Olmos R, González-Sagrado M, González ML, Ruiz MÁ, García-Talavera P, Gamazo C, Villanueva JG, Cobo A, de Luis D. Contribution of ^{111}In-pentetreotide SPECT/CT imaging to conventional somatostatin receptor scintigraphy in the detection of neuroendocrine tumours. Nucl Med Commun. 2015 Mar;36(3):251-9.

120 (119. Pfeifer A, Knigge U, Binderup T, Mortensen J, Oturai P, Loft A, Berthelsen AK, Langer SW, Rasmussen P, Elema D, von Benzon E, Højgaard L, Kjaer A. 64Cu-DOTATATE PET for Neuroendocrine Tumors: A Prospective Head-to-Head Comparison with 111In-DTPA-Octreotide in 112 Patients. J Nucl Med. 2015 Jun;56(6):847-54

121 (120. Perri M, Erba P, Volterrani D, Lazzeri E, Boni G, Grosso M, Mariani G. Octreo-SPECT/CT imaging for accurate detection and localization of suspected neuroendocrine tumors. Q J Nucl Med Mol Imaging. 2008 Dec;52(4):323-33

122 (121. Wong KK, Cahill JM, Frey KA, Avram AM. Incremental value of 111-in pentetreotide SPECT/CT fusion imaging of neuroendocrine tumors. Acad Radiol. 2010 Mar;17(3):291-7.

123 (122.Poeppel TD, Binse I, Petersenn S, Lahner H, Schott M, Antoch G, Brandau W, Bockisch A, Boy C. 68Ga-DOTATOC versus 68Ga-DOTATATE PET/CT in functional imaging of neuroendocrine tumors. J Nucl Med. 2011 Dec;52(12):1864-70.

124 (123.Velikyan I, Sundin A, Sörensen J, Lubberink M, Sandström M, Garske-Román U, Lundqvist H, Granberg D, Eriksson B. Quantitative and qualitative intrapatient comparison of 68Ga-DOTATOC and 68Ga-DOTATATE: net uptake rate for accurate quantification. J Nucl Med. 2014 Feb;55(2):204-10

125 (124.Yang J, Kan Y, Ge BH, Yuan L, Li C, Zhao W. Diagnostic role of Gallium-68 DOTATOC and Gallium-68 DOTATATE PET in patients with neuroendocrine tumors: a meta-analysis. Acta Radiol. 2014 May;55(4):389-98.

126 (125. Johnbeck CB, Knigge U, Kjær A. PET tracers for somatostatin receptor imaging of neuroendocrine tumors: current status and review of the literature. Future Oncol. 2014 Nov;10(14):2259-77

127 (126.Geijer H, Breimer LH. Somatostatin receptor PET/CT in neuroendocrine tumours: update on systematic review and meta-analysis. Eur J Nucl Med Mol Imaging. 2013 Oct;40(11):1770-80

128 (127. Treglia G, Castaldi P, Rindi G, Giordano A, Rufini V. Diagnostic performance of Gallium-68 somatostatin receptor PET and PET/CT in patients with thoracic and gastroenteropancreatic neuroendocrine tumours: a meta-analysis. Endocrine. 2012 Aug;42(1):80-7.
129 (128. Kayani I, Conry BG, Groves AM, Win T, Dickson J, Caplin M, Bomanji JB. A comparison of 68Ga-DOTATATE and 18F-FDG PET/CT in pulmonary neuroendocrine tumors. J Nucl Med. 2009 Dec;50(12):1927-32
130 (129. Squires MH 3rd, Volkan Adsay N, Schuster DM, Russell MC, Cardona K, Delman KA, Winer JH, Altinel D, Sarmiento JM, El-Rayes B, Hawk N, Staley CA 3rd, Maithel SK, Kooby DA. Octreoscan Versus FDG-PET for Neuroendocrine Tumor Staging: A Biological Approach. Ann Surg Oncol. 2015 Jul;22(7):2295-301.

131 (130. Boellaard R, Delgado-Bolton R, Oyen WJ, Giammarile F, Tatsch K, Eschner W, Verzijlbergen FJ, Barrington SF, Pike LC, Weber WA, Stroobants S, Delbeke D, Donohoe KJ, Holbrook S, Graham MM, Testanera G, Hoekstra OS, Zijlstra J, Visser E, Hoekstra CJ, Pruim J, Willemsen A, Arends B, Kotzerke J, Bockisch A, Beyer T, Chiti A, Krause BJ; European Association of Nuclear Medicine (EANM). FDG PET/CT: EANM procedure guidelines for tumour imaging: version 2.0. Eur J Nucl Med Mol Imaging. 2015 Feb;42(2):328-54.

132 (131. Velikyan I, Sundin A, Eriksson B, Lundqvist H, Sörensen J, Bergström M, Långström B. In vivo binding of [68Ga]-DOTATOC to somatostatin receptors in neuroendocrine tumours--impact of peptide mass. Nucl Med Biol. 2010 Apr;37(3):265-75.
133 (132. Haug AR, Rominger A, Mustafa M, Auernhammer C, Göke B, Schmidt GP, Wängler B, Cumming P, Bartenstein P, Hacker M. Treatment with octreotide does not reduce tumor uptake of (68)Ga-DOTATATE as measured by PET/CT in patients with neuroendocrine tumors. J Nucl Med. 2011 Nov;52(11):1679-83.

134 (133.Pettinato C, Sarnelli A, Di Donna M, Civollani S, Nanni C, Montini G, Di Pierro D, Ferrari M, Marengo M, Bergamini C. 68Ga-DOTANOC: biodistribution and dosimetry in patients affected by neuroendocrine tumors. Eur J Nucl Med Mol Imaging. 2008 Jan;35(1):72-9.

135 (134. Radiation dose to patients from radiopharmaceuticals (addendum 2 to ICRP publication 53). Ann ICRP. 1998;28(3):1-126.

136 (135. Gibril F, Reynolds JC, Chen CC, Yu F, Goebel SU, Serrano J, Doppman JL, Jensen RT. Specificity of somatostatin receptor scintigraphy: a prospective study and effects of false-positive localizations on management in patients with gastrinomas. J Nucl Med. 1999 Apr;40(4):539-53

137 (136. Castellucci P, Pou Ucha J, Fuccio C, Rubello D, Ambrosini V, Montini GC, Pettinato V, Malizia C, Lodi F, Fanti S. Incidence of increased 68Ga-DOTANOC uptake in the pancreatic head in a large series of extrapancreatic NET patients studied with sequential PET/CT. J Nucl Med. 2011 Jun;52(6):886-90.

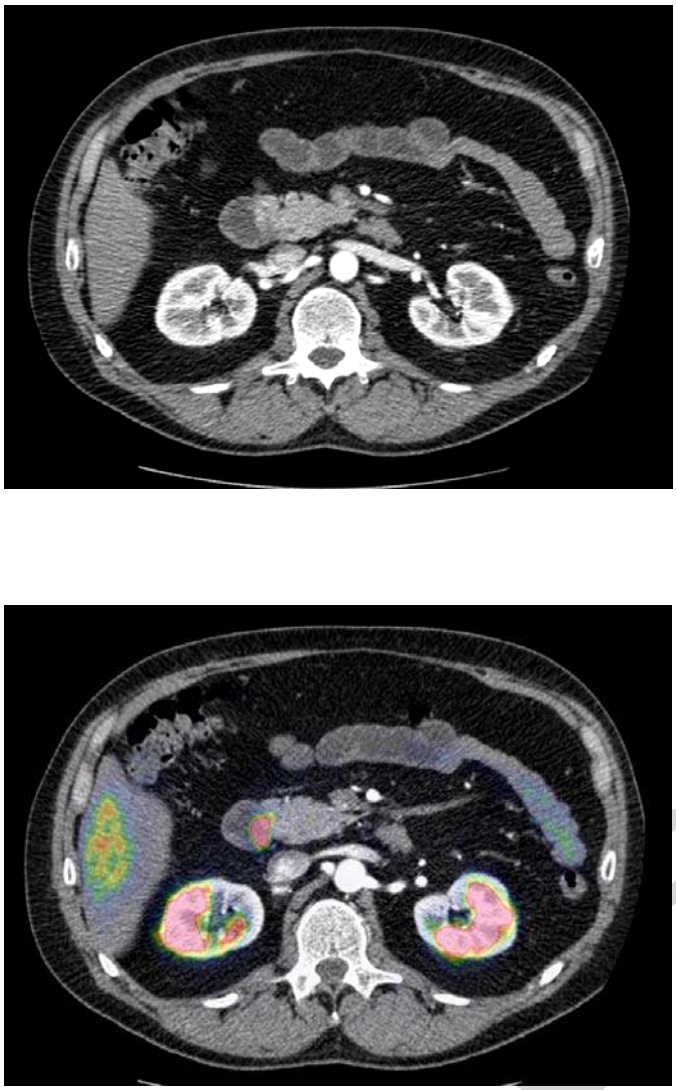

Figure 1. A. Transverse i.v. contrast-enhanced CT in the arterial phase showing a duodenal NET contrast-enhancing NET (arrow) surrounded by water in the duodenum. B. This tumor was also depicted by ^{68}Ga-DOTATOC-PET/CT shown in the PET/CT-fusion image.

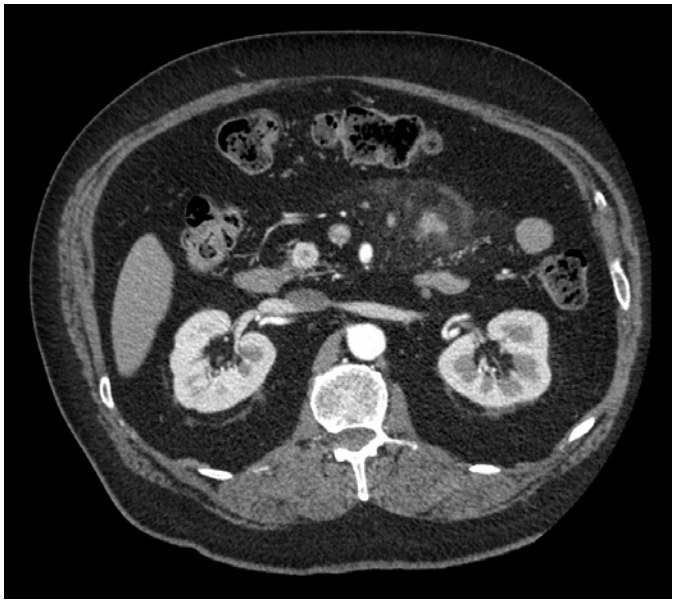

Figure 2. Transverse i.v. contrast-enhanced CT in the arterial phase showing a hypervascular pancreatic NET (arrow) in the uncinate process of the pancreas.

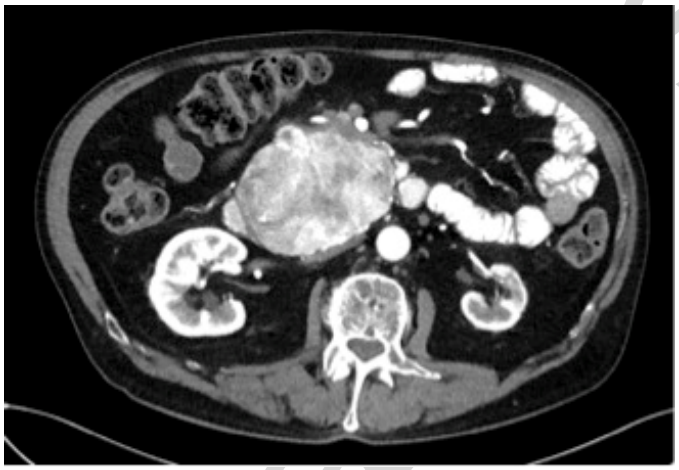

Figure 3. Transverse i.v. contrast-enhanced CT in the arterial phase showing a hypervascular pancreatic NET (glucagonoma) in the pancreatic head.

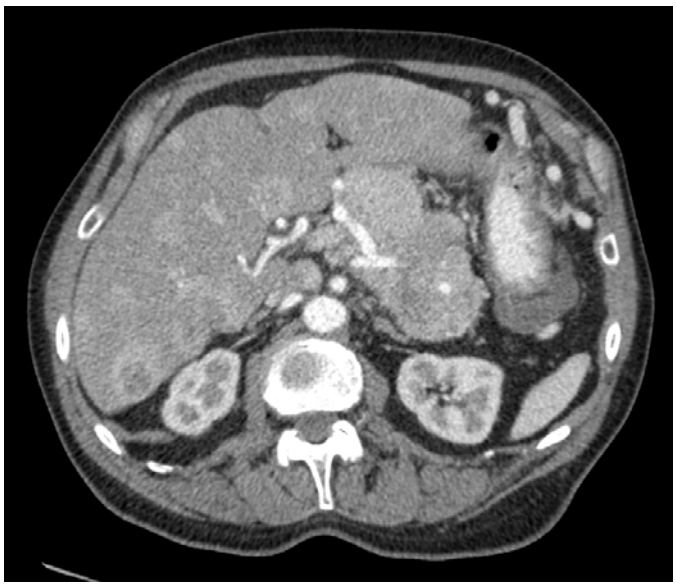

Figure 4. Transverse i.v. contrast-enhanced CT in the arterial phase showing a hypovascular pancreatic NET (arrow) in the pancreatic body. There is tumor encasement of the spleenic and main hepatic artery (arrows).

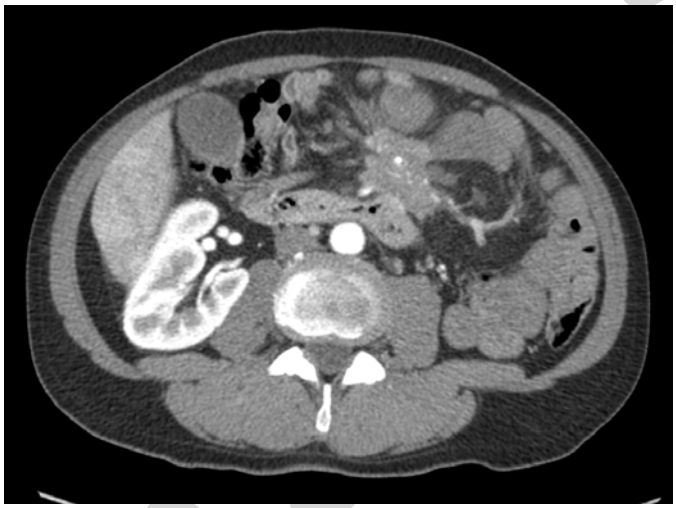

Figure 5. Transverse i.v. contrast-enhanced CT in the arterial phase showing a mesenteric metastasis from a small intestinal NET with typical central calcification (short arrow) and desmoplastic reaction with stranding of the surrounding mesenteric fat.

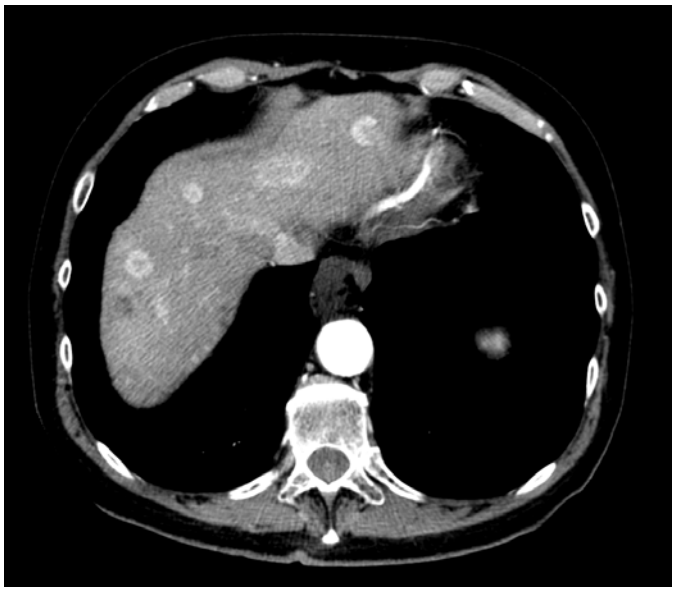

Figure 6. Transverse i.v. contrast-enhanced CT in the arterial phase showing hypervascular (bright) liver metastases.

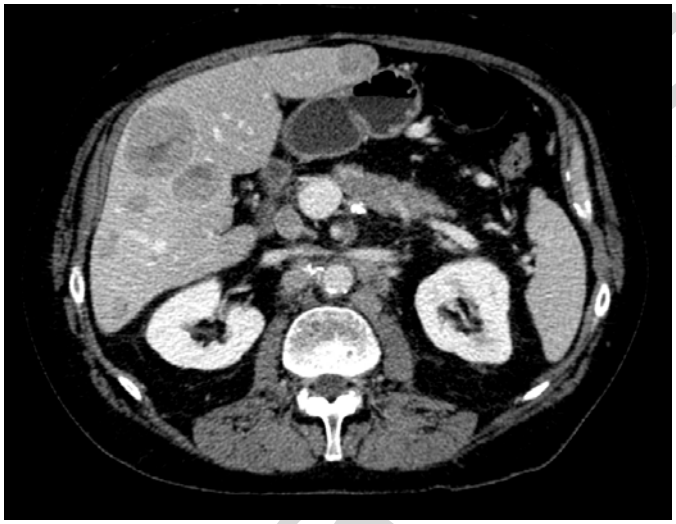

Figure 7. Transverse i.v. contrast-enhanced CT in the venous phase showing hypovascular (dark) liver metastases.

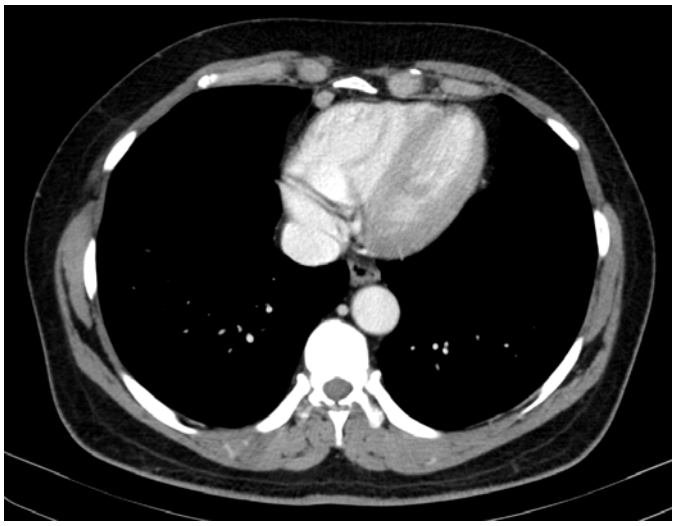

Figure 8. Transverse i.v. contrast-enhanced CT in the venous phase showing a lymph node metastasis from a small intestinal NET in the right lower-ventral thorax adjacent to the heart (arrow).

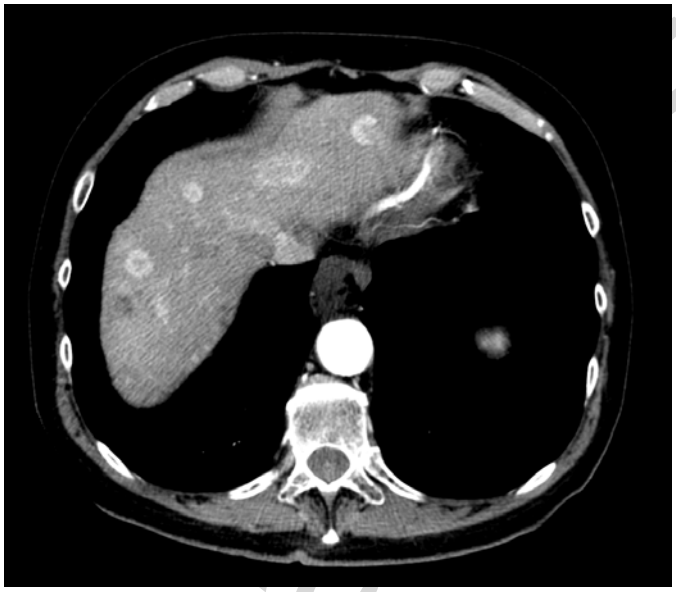

Figure 9. Transverse i.v. contrast-enhanced CT in the arterial phase showing a retrocrural lymph node metastasis from a small intestinal NET (long arrow) and peritoneal carcinomatosis, in this patient a nodular type with several small rounded tumor deposits in the ventral part of the abdomen (short arrows). There is also a hypervascular (bright) liver metastasis.

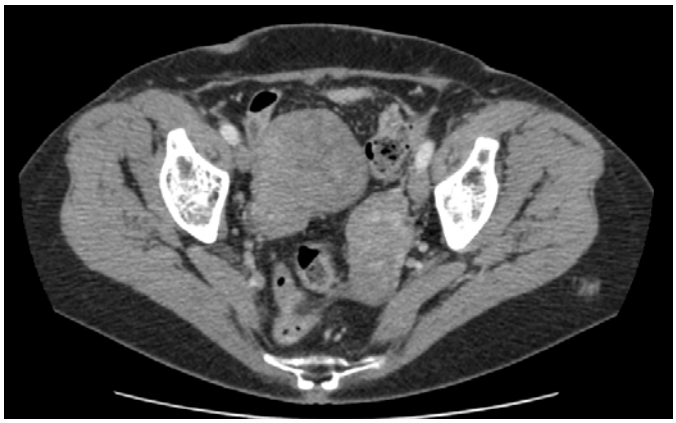

Figure 10. Transverse i.v. contrast-enhanced CT in the venous phase showing bilateral ovarian metastases (arrows) from a small intestinal NET.

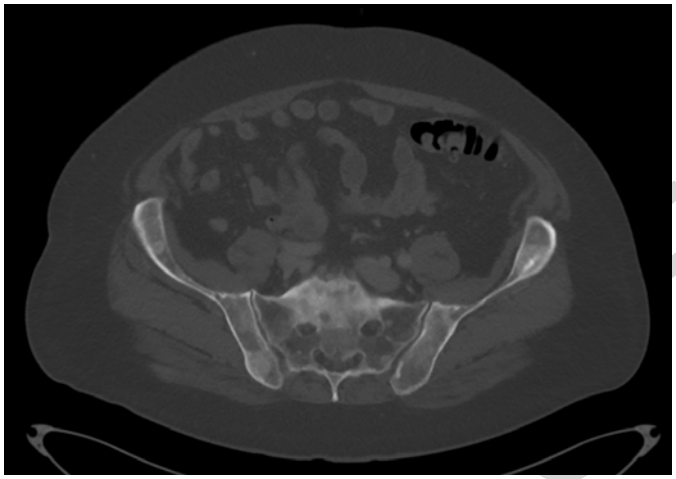

Figure 11. Transverse i.v. contrast-enhanced CT in the venous phase (bone window setting) showing multiple sclerotic (bright) bone metastases in the pelvis and sacrum.

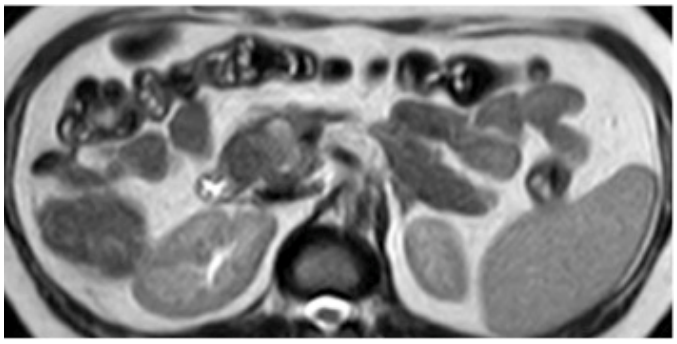

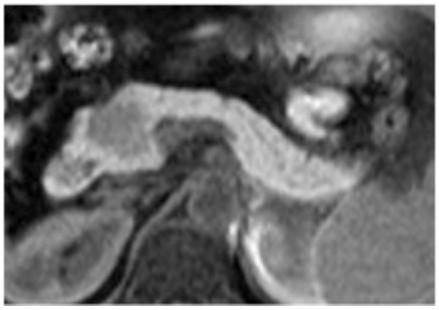

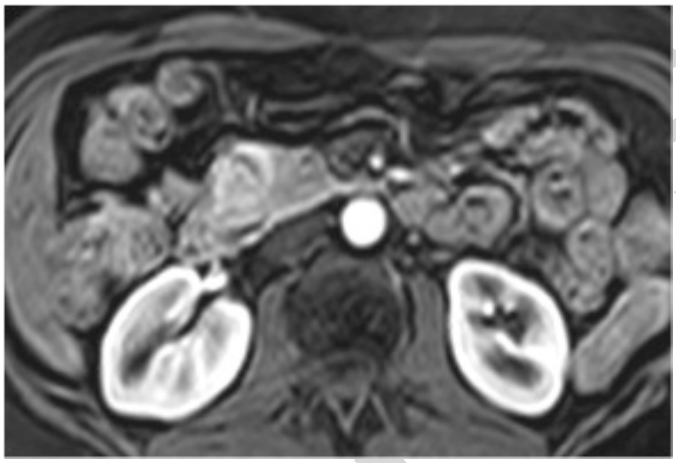

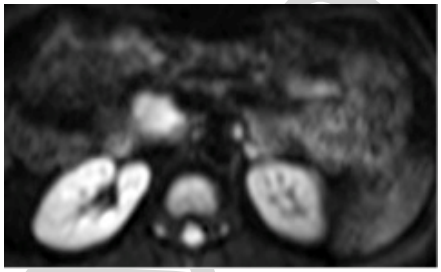

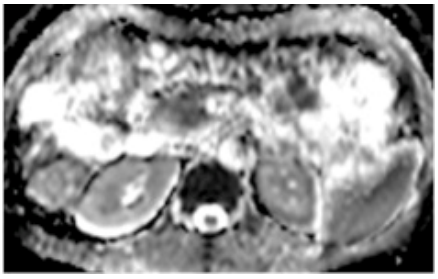

Figure 12. Poorly differentiated pancreatic NET in the head. A. Transverse T2-weighted MRI showing the pNET slightly hyperintense (arrow). B The pNET is markedly hypointense in the T1-weighted MRI. C. Transverse T1weighted gadolinium contrast-enhanced MRI in the arterial phase. D. Transverse diffusion-weighted MRI (DW MRI) b 800 showing the high signal of the pNET (arrows). E. DW MRI, attenuation diffusion cartography (ADC), showing a very low signal, measured at a value of 1, the lesion was grade 3, poorly differentiated.

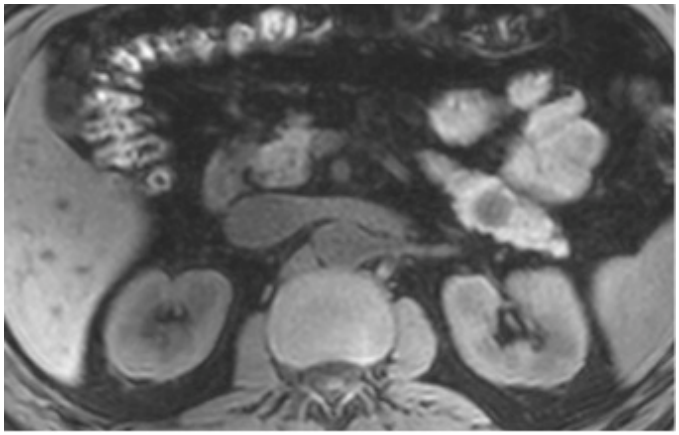

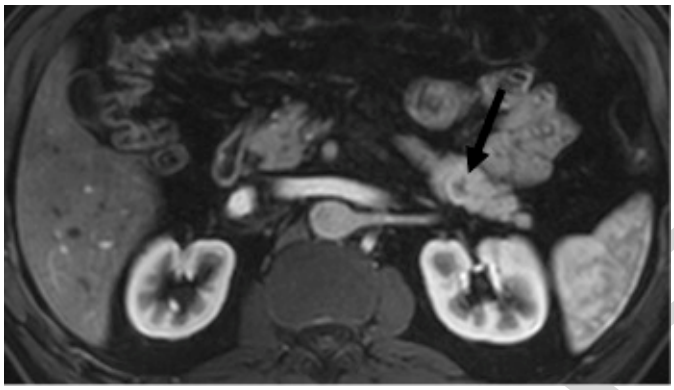

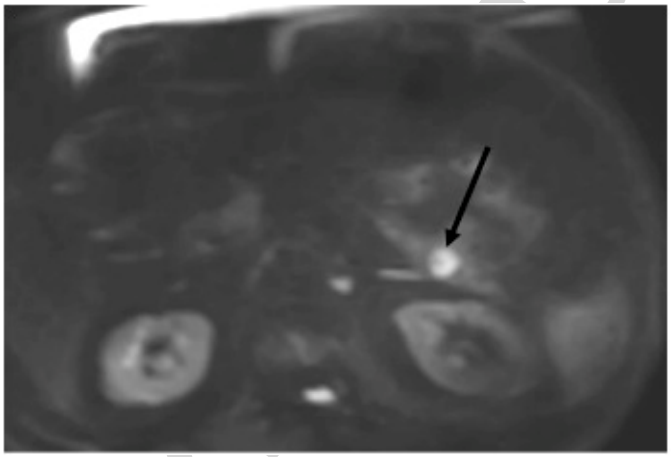

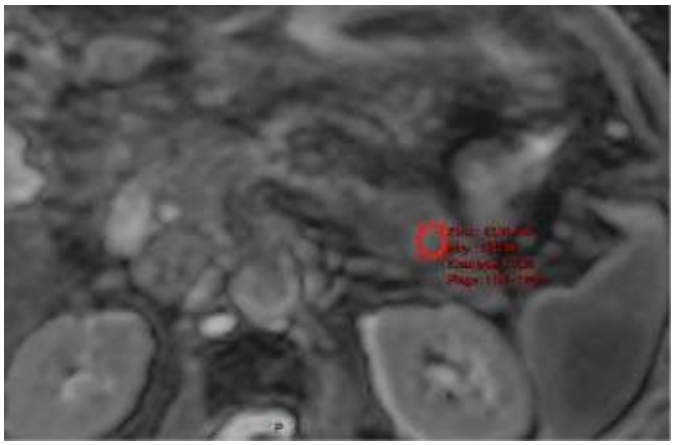

Figure 13. Benign G1 pNET.A. Transverse T1-weighted pre-contrast MRI, showing a hypointense rounded well-delineated tumor in the tail of the pancreas.. B. Transverse T1-weighted i.v. gadolinium contrast-enhanced MRI in the arterial phase, showing a slight peripheral contrast-enhancement of the tumor (arrow). C. DW MRI, b 800 showing the pNET slightly hyperintense (arrow). D. DW MRI, apparent diffusion coefficient (ADC) map, showing an intermediate ADC value of 1,54, in favor of a benign lesion.

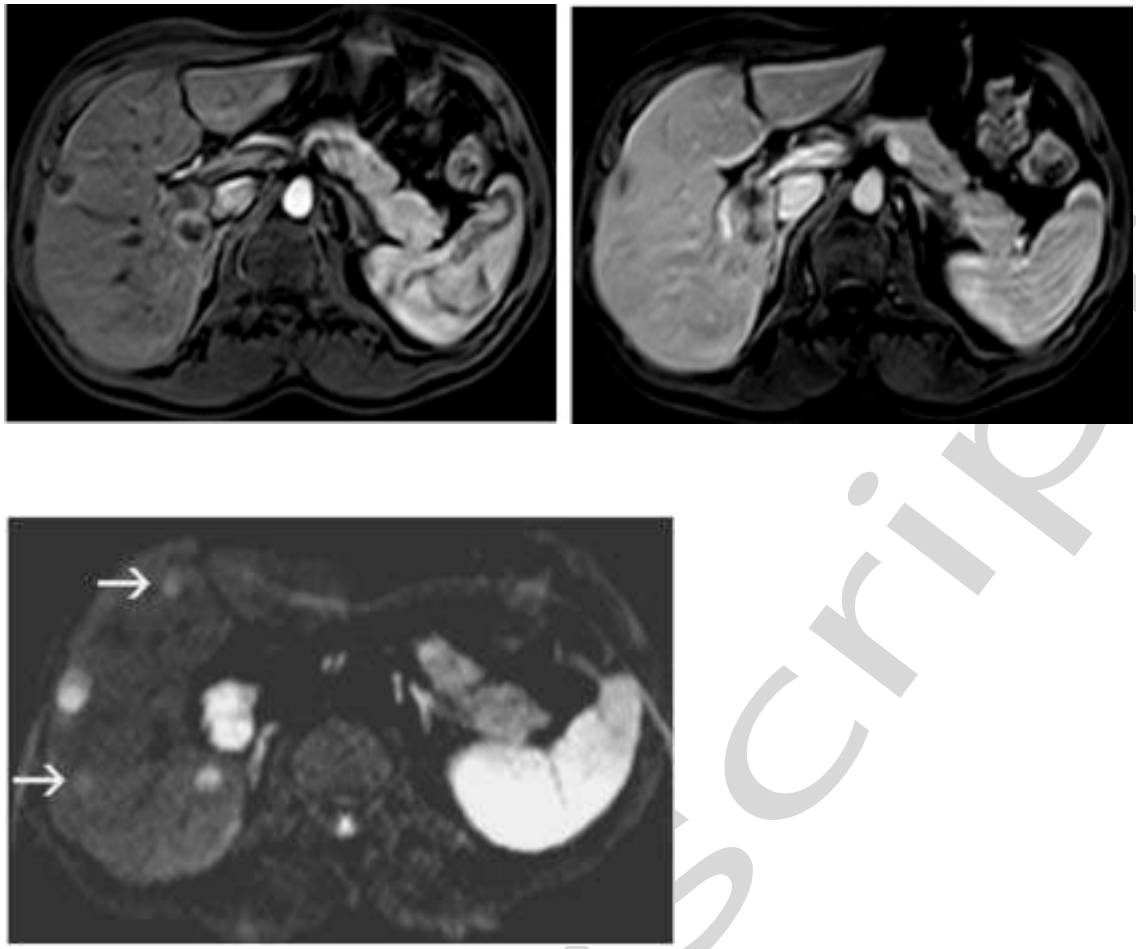

Figure 14. NET liver metastases. A & B. Transverse T1-weighted gadolinium contrast-enhanced MRI in the arterial (A) and venous (B) phase, showing 3 liver metastases. C. DW MRI (b 800), showing 3 more hyperintense liver metastases (arrows).

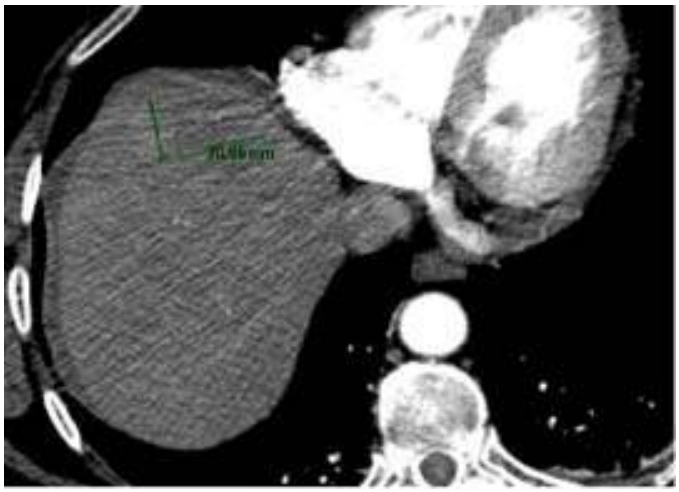

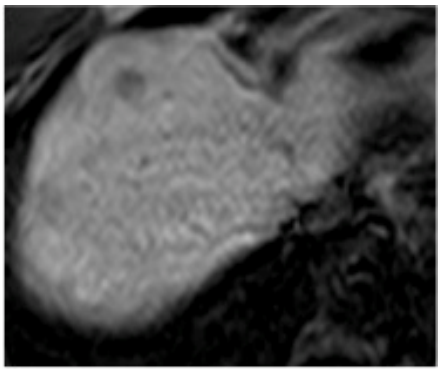

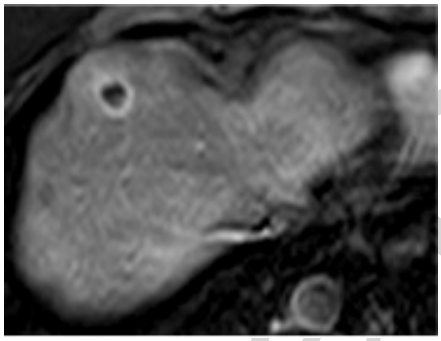

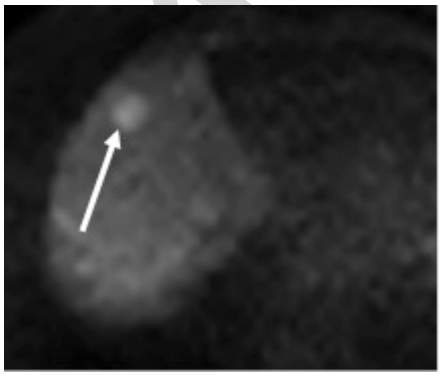

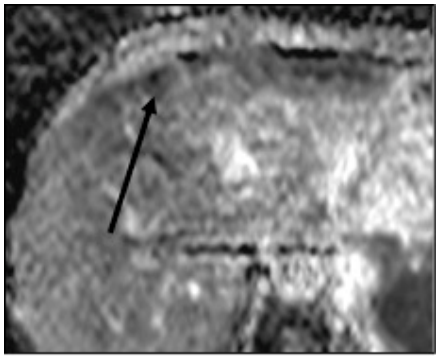

Figure 15. Typical liver metastasis. A. I.v. contrast-enhanced MDCT in the arterial phase showing a slight enhancement in the metastasis. B & C. Transverse T1-weighted (B) and T1-weighted gadolinium contrast-enhanced T1-weighted MRI in the arterial phase (C) showing an hypointense metastasis with rim enhancement. D & E. Transverse DW MRI (b 600), showing a hyperintense metastasis (white arrow), with a very low ADC appearing as a dark area (black arrow).

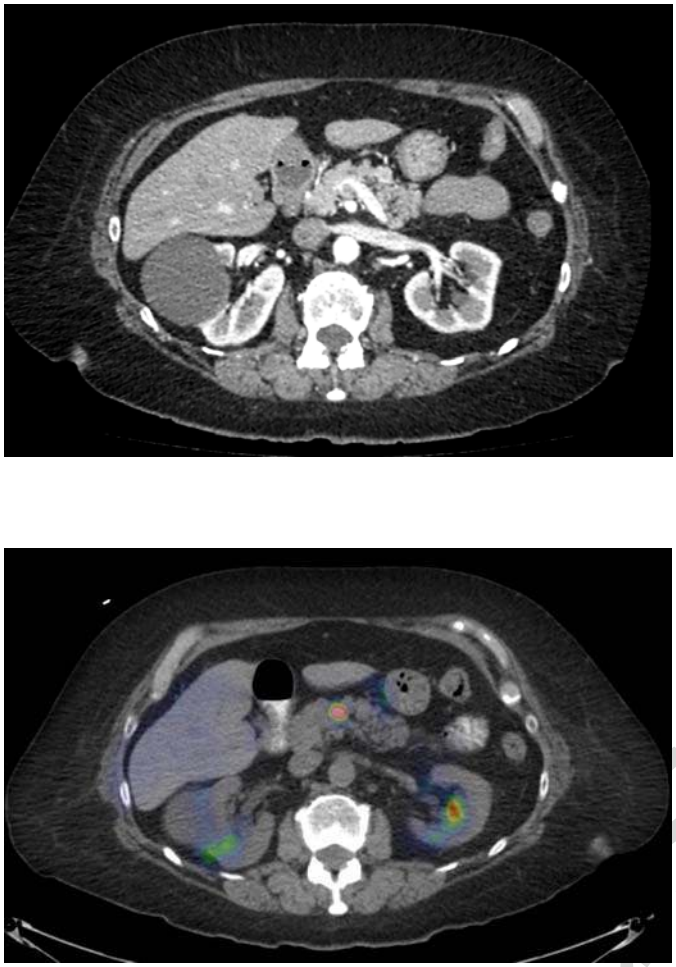

Figure 16. ^{68}Ga-DOTATOC-PET/CT A. Transverse i.v. contrast-enhanced CT in the arterial phase showing a hypervascular pancreatic NET in the ventral aspect of the pancreatic body. B. ^{68}Ga-DOTATOC-PET/CT fusion image showing a high tracer uptake in the tumor.

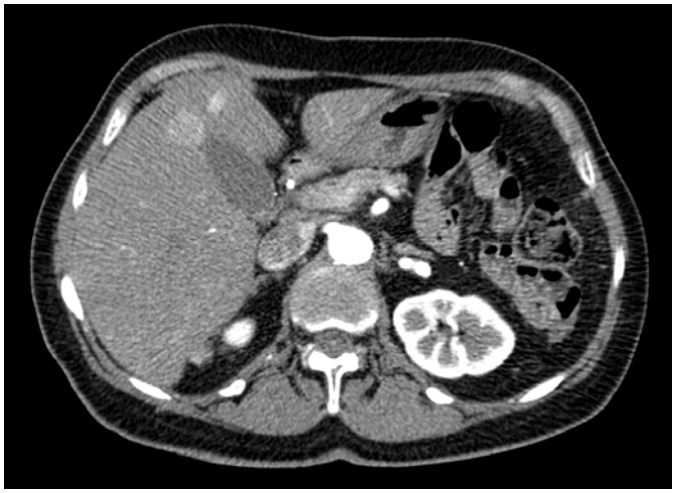

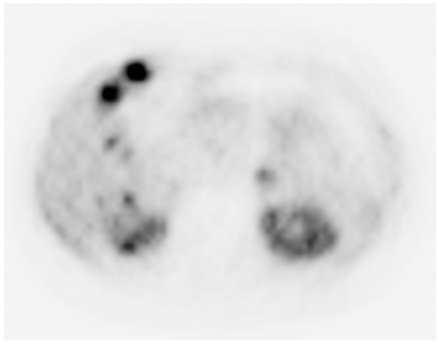

Figure 17. ^{68}Ga-DOTATOC-PET/CT A. Transverse i.v. contrast-enhanced CT in the arterial phase showing hypervascular livermetastases from a pancreatic NET. B. ^{68}Ga-DOTATOC-PET/CT showing a high tracer uptake in the liver metastases in the ventral aspect of the liver and showing additional small liver metastases (arrows). Bilaterally the tracer uptake in the kidneys are also apparent as in the physiological tracer accumulation in the left adrenal (short arrow).

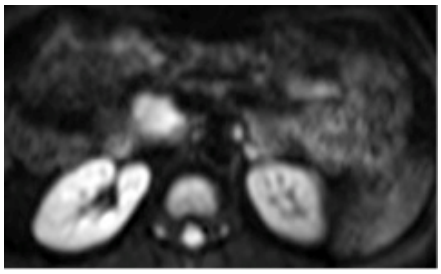

Figure 18. ^{68}Ga-DOTATOC-PET/CT Maximum Intensity Projection (MIP) volume showing multiple bone metastases, liver metastases and abdominal lymph node metastases in a patient with pancreatic NET (resected). Note that the lymph node metastases are very small similar to many of the bone metastases that were not diagnosed at CT.

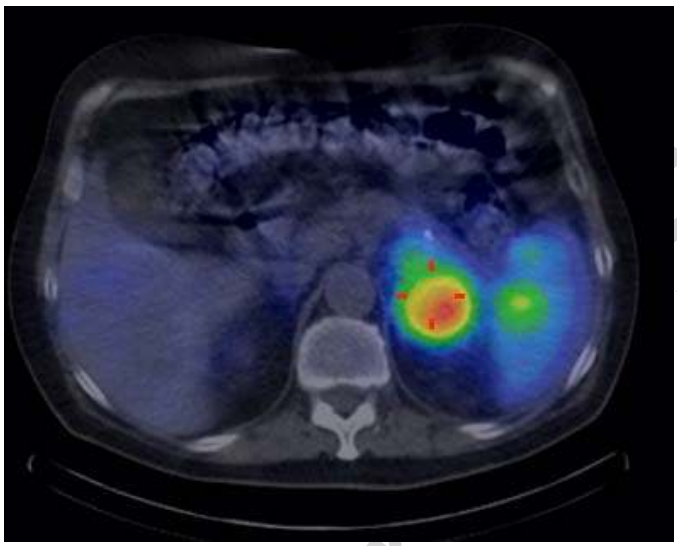

Figure 19. Somatostatin receptor scintography; transversal SPECT/CT fusion image 24h after injection of OctreoScan™ showing a high tracer uptake in the pancreatioc NET in the tip of the pancreatic tail.

Table 1. Data in the literature on the sensitivity, specificity and detection rate for NET diagnosis by CT.

Table 1. CT diagnosis of NETs

Type of NET	Sensitivity mean (range)	Specificity mean (range)	Detection rate mean (range)	Patients/ Studies	Reference
NET disease	82% (77–85)	86% (71–85)		253/4	3-6
Pancreatic NET	82% (67–96)	96%		119/2	10-11
Liver metastases			79% (73–94)	79/3	7-9
	84% (75–100)	92% (83–100)		342/5	3, 12-15
Extrahepatic abdominal soft tissue metastases	70% (60–100)	96% (87–100)		451/6	3, 12-15, 17
Bone metastases	61% (46-80)	99% (98-100)		337/3	3, 18,19
CT enteroclysis for SI-NETs	50% 85%	25% 97%		8/1 [a]219/1	20 21

[a] Out of 219 patients included in the study there were 19 subjects with SI-NETs.

Table 2. Data in the literature on the sensitivity, specificity and detection rate for NET diagnosis by MRI.

Table 2. MRI diagnosis of NETs

Type of NET	Sensitivity mean (range)	Specificity mean (range)	Detection rate mean (range)	Patients/ Studies	Reference
Gastrinoma	70%			122/1	28
Pancreatic NET	79% (54-100)	100 %	76% (61–95)	258/7	11, 29-34
Liver metastases	75% (70–80)	98%		200/2	40, 41
Carcinomatosis			88% (81-91)	72/2	42, 43

Table 3. Data in the literature on the sensitivity, specificity and detection rate for NET diagnosis by US, EUS, IOUS and CEUS.

Table 3. US, EUS, IOUS and CEUS diagnosis of NETs

Type of NET and US method	Sensitivity mean (range)	Specificity mean (range)	Detection rate mean (range)	Number of patients/studies	Reference
pNETs					
US			39% (17–76)	250/6	61-66
EUS			86% (75-97)	220/9	9, 62, 63, 66, 70-74
	86% (82-93)	92% (86-95)		149/3	67-69
IOUS			92% (74–96)	127/4	64, 66, 75, 76
Insulinoma					
EUS			86% (57–100)	250/12	63, 64, 72, 77-85
IOUS			92% (84–100)	264/9	66, 75, 76, 86-91
Duodenal tumors and lymph node metastases					
US			18%	25/1	66
EUS			63%	59/2	66 72
Liver metastases					
US	88%	95%		131/1	12
CEUS	82%			48/1	92

Table 4. Data in the literature on the detection rate for NET diagnosis by SRS using pentetreotide.

[b]**Detection rate**	**Tumor type**	**Reference**
High >75%		
	Primary Gastroenteropancreatic NETs	14
	Gastrinomas	15-16
	Nonfunctioning pancreatic NETs	17-18
	Functioning pancreatic NETs except insulinoma	17-18
	Carcinoids	19–22
	Paragangliomas	23–25
	Small cell lung cancer	26–29
	Meningiomas	30-31
Intermediate 40-75%		
	Insulinomas	17, 35
	Medullary thyroid carcinoma	36–38
	Differentiated thyroid carcinoma (including Hurthle cell carcinoma)	39–41
	Pheochromocytoma	45

[b]Detection rate is patient- and lesion-based.

Table 5. Data in the literature on the sensitivity, specificity and detection rate for NET diagnosis by PET/CT with 68Ga-DOTA-somatostatin analogs. [C]CUP; Cancer with unknown primary tumor site

Table 5. [68]Ga-DOTA-somatostatin analog-PETCT diagnosis of NETs

Type of NET	Sensitivity mean (range)	Specificity mean (range)	Detection rate mean (range)	Patients/ Studies	Reference
NETs all types	92% (64-100)	88% (50-100)		416/10	125
NETs all types	92% (64-100)			2078/21	126
		95% (83-100)		1776/8	
NETs all types	88% (70-100)			2105/22	127
NETs all types	93% (72-100)			567/16	128
		90% (67-100)		325/6	
Duodenopancreatic NETs	92%	83%		19/1	126
Gastrinomas	68%			21/1	126
[C]NET CUP	52% (36-60)			93/3	126
Bone metastases	97-100%	92-100%		95/2	126

Table 6. Pitfalls and causes of potential misinterpretation of positive results at SRS using pentetreotide.

Radiation pneumonitis
Accessory spleen
Focal collection of stools
Surgical scar tissue
Gallbladder uptake
Nodular goiter
Ventral hernia
Bacterial pneumonia
Respiratory infections
Common cold (nasal uptake)
Cerebrovascular accident
Concomitant granulomatous disease
Diffuse breast uptake
Adrenal uptake
Urine contamination
Concomitant second malignant tumor

Neuroendocrinology (*International Journal for Basic and Clinical Studies on Neuroendocrine Relationships*)
Journal Editor: Millar R.P. (Edinburgh)
ISSN: 0028-3835 (Print), eISSN: 1423-0194 (Online)
www.karger.com/NEN